1-1-2012

Fatigue and Crack-Growth in 7050-T7451 Aluminum Alloy under Constant- and Variable-Amplitude Loading

Justin Wayne Shaw

Fatigue and crack-growth in 7050-T7451 aluminum alloy under constant- and variable-amplitude loading

By

Justin Wayne Shaw

A Thesis
Submitted to the Faculty of
Mississippi State University
in Partial Fulfillment of the Requirements
for the Degree of Masters of Science
in Aerospace Engineering
in the Department of Aerospace Engineering

Mississippi State, Mississippi

August 2012

Fatigue and crack-growth in 7050-T7451 aluminum alloy under constant- and variable-amplitude loading

By

Justin Wayne Shaw

Approved:

James C. Newman, Jr. Professor of Aerospace Engineering Director of Thesis	Masoud Rais-Rohani Professor of Aerospace Engineering Committee Member
Rani W. Sullivan Associate Professor of Aerospace Engineering Committee Member	J. Mark Janus Associate Professor and Graduate Coordinator for Aerospace Engineering
Sarah A. Rajala Dean of the Bagley College of Engineering	

Name: Justin Wayne Shaw

Date of Degree: August 11, 2012

Institution: Mississippi State University

Major Field: Aerospace Engineering

Major Professor: James C. Newman, Jr.

Title of Study: Fatigue and crack-growth in 7050-T7451 aluminum alloy under constant- and variable-amplitude loading

Pages in Study: 54

Candidate for Degree of Masters of Science

Fatigue and crack-growth tests were conducted on 7050-T7451 aluminum alloy under a wide range of loading conditions. Crack-growth tests were conducted on compact, C(T), specimens under constant-amplitude loading, single-spike overloads, and a simulated aircraft spectrum loading. Fatigue tests were also conducted on single-edge-notch bend, SEN(B), specimens under constant-amplitude loading and three aircraft load spectra. The FASTRAN, life-prediction code, was used to make crack-growth predictions on the C(T) specimens; and to make fatigue-life calculations using a 12-micrometer initial flaw size at the center of the edge-notch on the SEN(B) specimens. The predictions agreed fairly well with most of the tests, except the model was unconservative on the single-spike overload tests and the severe spectrum Mini-TWIST+ Level 1 tests. The discrepancy was suspected to be caused by a low constraint factor and/or crack paths meandering around overload plastic zones. A roughness- and plasticity-induced crack-closure model would be needed to improve the model.

DEDICATION

The author dedicates this thesis to his family for encouraging him to pursue a college career in order to be the first person in his family to have a college degree.

ACKNOWLEDGEMENTS

The author would like to express his gratitude towards everyone in the Aerospace Engineering Department at Mississippi State University who helped to make this thesis possible. Special thanks are given to Dr. James Newman, Jr. for all the assistance and advice he provided during the course of this thesis. Also, special thanks is given to Dr. Yoshiki Yamada for his previous research on the 7050 aluminum alloy and Dr. Brett Zeigler for his training to use the servo-hydraulic test frames in the Fatigue and Fracture Laboratory. Gratitude is expressed towards the National Aeronautical and Space Administration, Langley Research Center, for providing 7050-T7451 aluminum alloy compact specimens and a forged block to machine the single-edge-notch bend specimens. The author would like to further express his gratitude to Dr. Balkrishna Annigeri from Pratt and Whitney Corporation and Mr. Nam Phan from the U.S. Navy (NAVAIR) for their financial support during his graduate career. Finally, special thanks are given to the other members of the thesis committee, Dr. Masoud Rais-Rohani and Dr. Rani Sullivan for their extensive review of this thesis.

TABLE OF CONTENTS

LIST OF TABLES

TABLE Page

LIST OF FIGURES

NOMENCLATURE

Symbol	Description
a_i	Initial crack depth
B	Thickness
BFS	Backface-strain
c	Crack length
c_i	Initial crack length
CMOD	Crack mouth opening displacement
CPCA	Compression precracking constant-amplitude
CPLR	Compression precracking load reduction
C(T)	Compact specimen
C_{1i}	Crack-growth coefficient for segment i
C_{2i}	Crack-growth power for segment i
$\frac{dc}{dN}$	Fatigue-crack-growth-rate
E	Modulus of elasticity
ESE(T)	Eccentrically loaded single edge-notch tension specimen
F	Boundary-correction factor
EDM	Electrical-discharge machining
HCF	High-cycle fatigue

h_n	Notch height
K_{cp}	Compressive stress-intensity factor during precracking
K_{Ie}	Elastic stress-intensity factor at failure
K_{max}	Maximum stress-intensity factor
K_{min}	Minimum stress-intensity factor
K_{op}	Crack tip opening stress-intensity factor
K_T	Stress concentration factor
LCF	Low-cycle fatigue
LEFM	Linear-elastic fracture mechanics
LT	Longitudinal orientation
N	Number of cycles
N_f	Fatigue life (cycles to failure)
OP0	0% compliance offset
OP1	1% compliance offset
OP2	2% compliance offset
P	Applied load
PICC	Plasticity-induced crack-closure
P_o	Crack-opening load
P_{max}	Maximum applied load
p, q	Constants selected to fit test data in the threshold or fracture regimes
R	Load (or stress) ratio
S	Applied stress
SEN(B)	Single-edge-notch bend specimen

SEN(T)	Single-edge-notch tension specimen
S_{max}	Maximum applied stress
S_{mf}	Mean flight stress
S_{min}	Minimum applied stress
S_o	Crack-opening stress
TL	Transverse orientation
W	Width
α	Tensile constraint factor
β	Compression constraint factor
ε	Strain
Δc	Crack extension
$\Delta\varepsilon$	Reduced strain
ΔK	Stress-intensity factor range
ΔK_{eff}	Effective stress-intensity factor range
ΔK_o	Effective threshold stress-intensity factor range
ΔK_{th}	Threshold stress-intensity factor range
ρ	Plastic zone size
ρ_{cp}	Compressive plastic zone size
σ_o	Flow stress
σ_{ult}	Ultimate tensile strength
σ_{ys}	Yield stress

CHAPTER I

INTRODUCTION

During the past three decades, a number of load-interaction models have been developed to correlate fatigue-crack-growth-rates and to predict fatigue-crack-growth and fatigue behavior under aircraft spectrum loading. These models have usually been based on plastic deformations that develop at the crack front, and have either been closure-based, or based on physical models of the crack-growth and closure process. In 1968, Elber observed fatigue-crack surfaces contact under cyclic tensile loading, and this observation and the crack-closure concept [1,2] began to explain many crack-growth characteristics under variable-amplitude loading. Since the discovery of plastically-induced crack closure, other closure mechanisms have been identified, such as roughness-, fretting-product-, and oxide-debris-induced closure. These mechanisms have greatly improved our understanding of the complex interactions that occur during fatigue-crack-growth under variable-amplitude loading [3]. Unfortunately, these other mechanisms have not been integrated into any of the major life-prediction codes, such as NASGRO [4], AFGROW [5], or FASTRAN [6].

Several numerical models of plasticity-induced crack closure have been developed to calculate crack-opening stresses under spectrum load histories, such as the FASTRAN (NASA) model by Newman [6,7] or the ESA/NLR STRIPY model by de Koning et al [8]. The STRIPY model is currently implemented into the NASGRO life-prediction software with two options that are the NASA model and ESA model. The

main difference between these two models is the constraint factor(s) that account for the three-dimensional stress states that develop around cracks.

The observation that small fatigue cracks can: (1) grow more rapidly than those predicted by linear-elastic fracture mechanics (LEFM) based on large-crack data, and (2) grow at stress-intensity factor (ΔK) levels below the large-crack threshold (ΔK_{th}), has attracted a substantial amount of attention in the past few decades [9-13]. Naturally-occurring small cracks are three-dimensional in nature. When approaching microstructual dimensions, these cracks are largely affected by crack shape (surface or corner cracks), enhanced crack-tip plastic strains due to microplasticity, local arrest at grain boundaries, and the lack of crack closure in the early stages of crack-growth. For aluminum alloys, such as those used in aircraft, the fatigue process has been shown to be primarily crack-growth from some microstructural feature, such as inclusion-particle clusters, voids, or pits [14-16]. In these studies, the FASTRAN model was applied to the growth of small cracks using continuum mechanics plasticity and small-crack data. The crack-closure transient or the lack of closure in the early stages of crack-growth has long been suspected as a leading cause of the small-crack effect. The influence of the microstructure is embodied in the crack-growth-rate data used to establish the crack-driving-force curve in the threshold and near-threshold regimes. The FASTRAN crack-closure model [6,7] has demonstrated the capability to model small-crack-growth behavior in a wide variety of materials and loading conditions [16-18]. This basic approach has been called Small-Crack Theory. However, difficulties still exist for materials and conditions that develop roughness- and debris-induced crack closure and for large-scale plastic deformations at holes or notches.

In the treatment of microstructurally, mechanically, and physically small cracks, two basic approaches have emerged to explain the rapid growth and deceleration of small cracks when compared to large-crack-growth behavior. The first is characterized by grain-boundary blocking and consideration of microstructural effects on small-crack-growth-rates [13,19]. The second one is a continuum mechanics approach that accounts for the effects of material nonlinearity on the crack-tip-driving force and crack-closure transients [20,21]. Recently, the generation of large-crack data using the traditional load-reduction test procedures has been shown by tests [22,23] to produce higher thresholds and slower fatigue-crack-growth-rates in the near-threshold regime. Therefore, some of the differences between small and large cracks may have been caused by this large-crack testing inconsistency.

It has been disputed that the calculation of ΔK for a small crack growing from an inclusion particle could be in error [24]. (For example, if a crack initiation occurs at a subsurface inclusion with subsequent breakthrough to the surface, a considerable elevation in ΔK is possible over that calculated from surface observations and a surface crack is growing in a vacuum.) The use of ΔK to characterize the growth of small cracks has proved to be convenient, but skepticism surrounds its universal application. Despite the concerns, research work on the growth of naturally initiated small cracks, notably by Lankford [25,26], the AGARD small-crack programs [14,15], and the NASA/CAE [16] study, have demonstrated the effectiveness of the ΔK concept for small-crack-growth.

Previous studies on the 7050-T7451 aluminum alloy [27-29] have identified that fatigue cracks develop very rough crack-surface profiles. These profiles cause very high crack-closure levels due to a combination of plasticity, roughness, and debris. Recently, tests [30] have been conducted on compact, C(T), specimens to generate crack-growth-

rate data from threshold to near fracture over a wide range in load ratios (R). New threshold testing methods, based on compression precracking, were used to generate the near threshold data. FASTRAN, a plasticity-induced crack-closure model, was used to correlate the fatigue-crack-growth data over a wide range in load ratios and rates from threshold to near fracture. A very low constraint factor, like plane-stress ($\alpha = 1.3$) conditions, had to be used in the model to account for the very high crack-closure levels. In addition, the crack-opening loads were measured during these tests using a local strain gage method to generate another effective stress-intensity (ΔK_{eff}) curve. These two curves only differed in the near threshold regime.

The purpose of this thesis was to conduct crack-growth and fatigue tests on the same batch of 7050-T7451 alloy, from reference 30, and to predict crack-growth and fatigue behavior under a wide variety of loading conditions. Fatigue-crack-growth tests were conducted on standard C(T) specimens under single-spike overloads and a simulated aircraft spectrum loading. In addition, fatigue tests on single-edge-notch bend, SEN(B), specimens were also conducted over a wide range in loading conditions including constant-amplitude and three aircraft spectra. All specimens were machined from a single forged block of 7050-T7451. However, no residual stresses were measured in the C(T) [30] and SEN(B) specimens. Three European standard spectra were used and modified to have only tension-tension loading by adding a mean load and maintaining the same load amplitudes and sequences. They were Mini-Falstaff [31,32] and Mini-TWIST Levels 1 and 3 [33,34]. The objective of this thesis was to evaluate the two different ΔK_{eff} curves on making crack-growth and fatigue-life predictions. Small-crack theory was used to make fatigue-life predictions on SEN(B) specimens using inclusion-particle sizes from the literature. For the C(T) specimens, comparisons were made on single-

spike overload and Mini-Falstaff+ spectrum loading tests. Some reasons for discrepancies among the measured and predicted results were discussed and recommendations for improved modeling were proposed.

CHAPTER II

SPECIMEN CONFIGURATIONS, TESTING PREPARATIONS AND METHODS, AND LIFE-PREDICTION ANALYSIS

2.1 Material Specifications

The 7050-T7451 aluminum alloy is used in many structural applications, such as engine, rotorcraft, and aircraft components. The aluminum alloy's material properties consisted of a yield stress (σ_{ys}) of 470 MPa, an ultimate tensile strength (σ_{ult}) of 525 MPa, and a modulus of elasticity (E) of 76 GPa. This material was obtained from the NASA Langley Research Center (LaRC). The C(T) specimens were previously machined by LaRC, and the SEN(B) specimens had to be machined from a single forge block of 7050-T7451 by Westmoreland Mechanical Testing and Research Company.

2.2 Specimen Configurations

In order to test and analyze the 7050-T7451 aluminum alloy, two different types of specimens were used. The C(T) specimen, shown in Figure 2.1, was used to generate fatigue-crack-growth-rate data [30] over a wide range of load ratios, the effects of a single-spike overload on crack-growth delay, and the crack-growth under an aircraft spectrum loading called Mini-Falstaff+ [35]. Some of these specimens had also been tested at LaRC using the American Society for Testing and Materials (ASTM) standard load-reduction (E-647) and the new compression precracking constant-amplitude (CPCA) loading procedures [30]. The specimens did not have the standard V-notch, but had an EDM (electrical-discharge machine) rectangular notch 10 mm long that was measured

from the pin-hole centerline. The total notch height (h_n) was 0.25 mm. The C(T) specimens had a width (W) of 50.8 mm and a thickness (B) of 6.35 mm. In addition, the edges of the pin-holes in the specimens were beveled to avoid or minimize undesired out-of-plane bending moments [30].

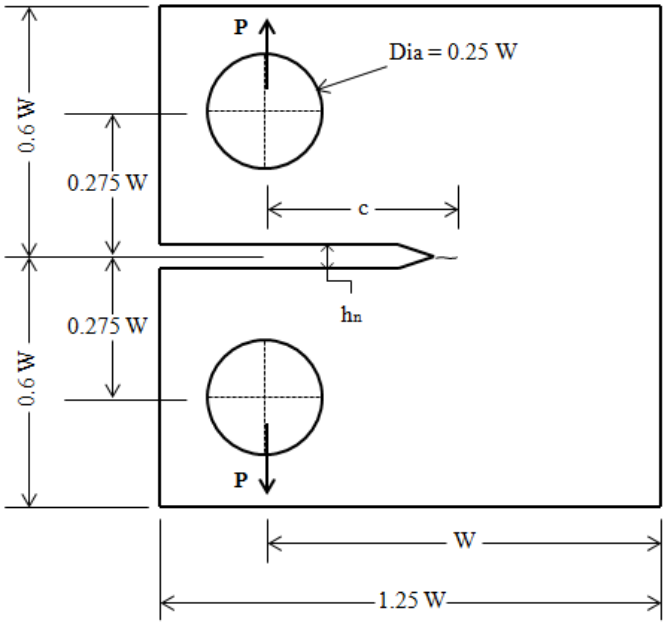

Figure 2.1 Compact, C(T), specimen

The SEN(B) specimen, shown in Figure 2.2, was developed to perform fatigue and small-crack tests using the equipment available in the Fatigue and Fracture Laboratory at Mississippi State University. A pin-loaded fatigue specimen was developed since all of the servo-hydraulic fatigue test frames use pin-loading clevises. The design of this specimen was focused on modifying the single-edge-notch tension, SEN(T), specimen that is a standard specimen used in the study of small cracks [16]. One major advantage for the SEN(B) specimen is a larger stress concentration at the notch, $K_T = 11.8$, compared to $K_T = 3.17$ for the SEN(T) specimen [16]. This makes it

possible to run a test at the same local notch-root stress level using a much lower applied load.

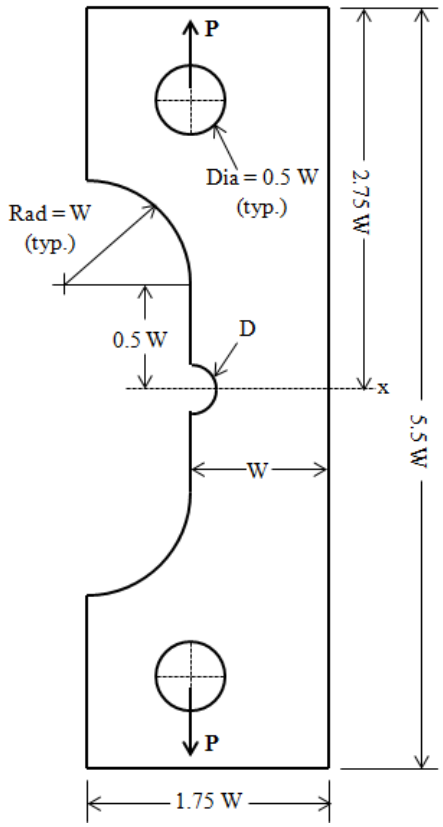

Figure 2.2 Single-edge-notch bend, SEN(B), specimen

2.3 Specimen Polishing

All large-crack fatigue-crack-growth tests required some way to measure crack length. These measurements were made by correlating backface strain readings to the crack length and were periodically compared to optical measurements of crack length made on one side of the specimen using a digital traveling microscope. Specimens were polished, either manually or electro-chemically, to help in making accurate optical measurements. When polishing, a thin layer of material is removed and the specimen surface is left with mirror finish. When manually polishing, surface residual stresses may

be introduced. For large-crack specimens, these residual stresses are negligible when compared to applied loads, but for fatigue tests, these residual stresses at the semi-circular notch are far too large to be ignored. Electro-chemical polishing is the better method for polishing fatigue specimens because it does not introduce residual stresses.

2.4 Hole Beveling

Zeigler [36] observed problems in fatigue-crack-growth tests with asymmetric crack fronts. It was determined that this behavior was most likely caused by the specimen experiencing an out-of-plane bending moment during the test. If pin-holes are not drilled precisely normal to the specimen surface for C(T) and SEN(B) specimens, one side of the specimen may be loaded slightly more than the other resulting in an unwanted out-of-plane bending moment. To minimize this bending moment, all of the specimen pin-holes were beveled by hand using a circular file. Zeigler's [36] inspection of fatigue surfaces on A36 eccentrically loaded single edge-notch tension ESE(T) specimens have shown that the process successfully removed most crack front asymmetry as seen in Figure 2.3 [36].

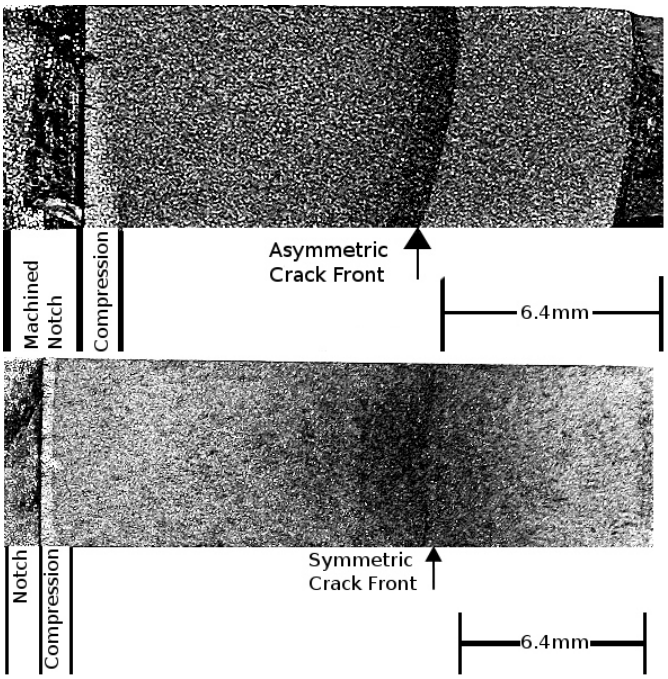

Figure 2.3 Crack surfaces of A36 ESE(T) specimens with non-beveled and beveled pin-holes

2.5 Testing Methods

All tests were performed using servo-hydraulic fatigue test frames. During each test, it was necessary to gather data about crack length, crack opening load, and applied load.

2.5.1 Crack Length Monitoring

For all fatigue-crack-growth tests performed, it was important to have accurate measurements, both digital and optical, of crack length at regular intervals. Optical measurements were performed manually using a traveling optical microscope. This method is accurate but collecting data at regular intervals becomes impractical, especially for tests that last several days. The optical measurements represent the crack length at the surface but cannot provide information about the crack length in the specimen interior. For this reason, all large-crack tests were monitored using a digital crack monitoring

system. This system actively measures strains at a constant location on the specimen and uses strain measurement calibrations to calculate a crack length. Most digital crack monitoring systems use one of two types of gages: crack mouth opening displacement (CMOD) gages or backface strain (BFS) gages.

CMOD gages are popular for being accurate and reusable but the gage applies a small tensile load at the crack mouth. For tests in which the applied loads are small, the gage force has significant influence on the crack-growth behavior, which must be accounted for during data analysis. For this reason, all fatigue-crack-growth tests used a digital crack monitoring system with a BFS gage. The BFS gage has essentially no effects on the crack-growth behavior. In this work, all tests were monitored using a BFS gage. The crack length calculations based on these gage readings were regularly compared to optical measurements to ensure that the collected crack length measurements were accurate.

2.5.2 Monitoring Applied Loads

The loads applied by the servo-hydraulic fatigue test frame were monitored using a load cell. The choice of load cell for each test was based on the magnitude of the load being applied. Every load cell has a limit load and resolution, and cells with lower limit loads have a higher resolution. For this reason, it is best to use a load cell with a limit as close as possible to the maximum expected load. For the testing described in this thesis, either a 5 kN or 25 kN load cell was used.

2.5.3 Compression Precracking

All C(T) specimens have a machined notch, which is not representative of a crack. In order to induce a physical crack in the specimen, the notch must be precracked

before testing can begin; however, cyclic precracking loads can be much larger than the desired cyclic test load. One solution to this problem is to start the precracking with a load large enough to initiate a crack and then gradually reduce the load after the crack has formed. Unfortunately, this results in a large plastic zone with compression residual stresses in front of the crack tip, which could potentially cause premature crack closure during testing and may result in inaccurate crack-growth behavior measurements.

An alternative method is to precrack using cyclic compressive loads. Applying compressive loads to a machined notch can result in the initiation of a crack resulting from tensile residual stresses in the plastic zone at the notch as seen in Figure 2.4 [36]. These local tensile stresses will eventually initiate a crack even if the maximum applied load is compressive. After a crack is initiated, cyclic tensile loads can be applied to grow the crack. Once the crack has grown out of the influence of the precracking residual stress field, the crack-growth-rate data is valid.

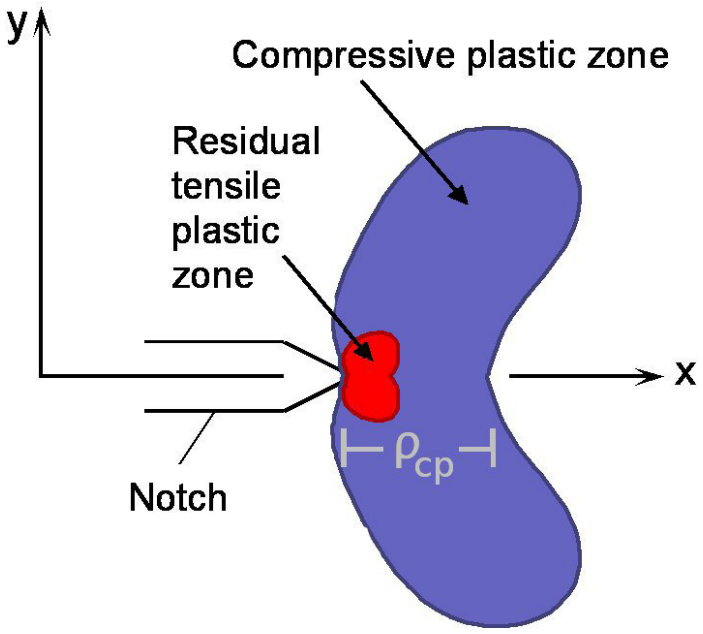

Figure 2.4 Plastic zone at the notch tip caused by cyclic compressive loading

It has been stated by Yamada [37] that the crack extension needed to grow out of the influence of precracking can be calculated using Equation (2.1) where $\gamma = 2$, Δc is the crack extension, R is the load ratio, and ρ_{cp} is the compressive plastic zone size. ρ_{cp} can be calculated with Equation (2.2) where K_{cp} is the stress-intensity factor for the cyclic maximum compressive load and σ_o is the flow stress for the material. To be more conservative, $\gamma = 3$ has been previously used in testing.

$$\Delta c = \gamma(1 - R)\rho_{cp} \tag{2.1}$$

$$\rho_{cp} = \frac{\pi}{8}\left(\frac{K_{cp}}{\sigma_o}\right)^2 \tag{2.2}$$

CPCA testing, shown in Figure 2.5(a), began with cyclic compressive loading followed by constant-amplitude tensile cyclic loading. In the event that the crack failed to grow at the applied tensile loading, the load was increased by 5%. Compression precracking load reduction (CPLR) testing, shown in Figure 2.5(b), began with cyclic compressive loading followed by constant-amplitude tensile cyclic loading until the crack extension necessary to ensure stable fatigue-crack-growth was achieved followed by load reduction.

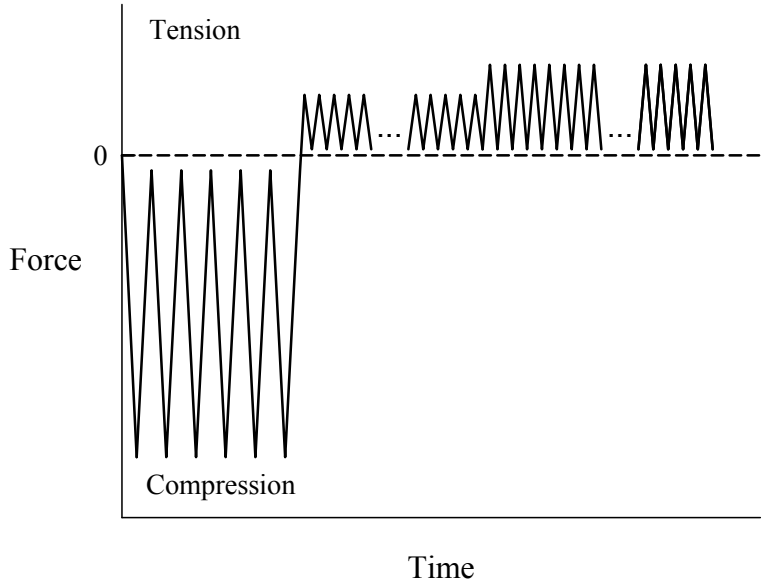

(a) Compression precracking constant-amplitude (CPCA) loading sequence

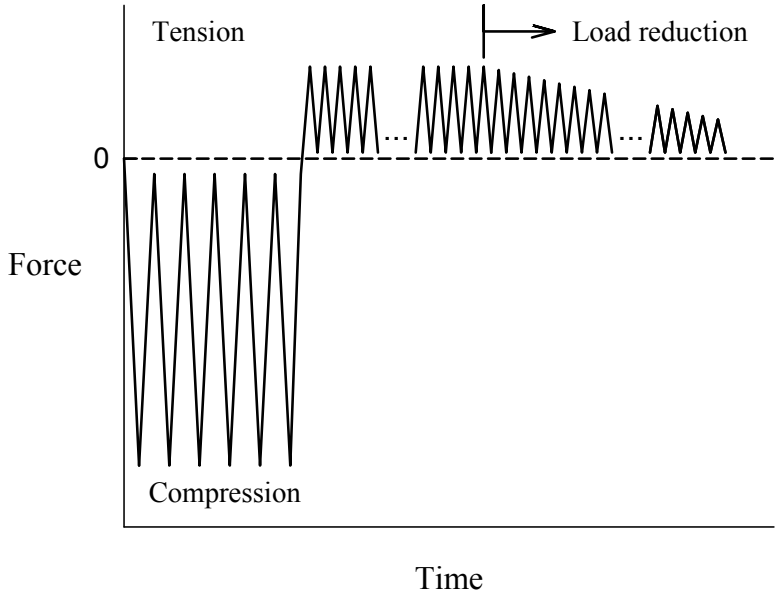

(b) Compression precracking load reduction (CPLR) loading sequence

Figure 2.5 Standard CPCA and CPLR load sequences

2.6 FASTRAN - A Fatigue-Crack-Growth Life-Prediction Code

FASTRAN 3.82sp is a life-prediction code based on the crack-closure concept and the modified Dugdale [38] or strip-yield model. (FASTRAN input user guide is presented in Appendix A). The code is used to predict crack length against cycles from a

specified initial crack size to failure for many common crack configurations found in structural components. The code has also been used to predict the fatigue behavior of some materials including aluminum alloys, steels, and titanium alloys, where inclusion particles or voids cause fatigue failures from the growth of small cracks. The life-prediction method used in FASTRAN is built around an analytical crack-closure model. The model is based on plasticity-induced fatigue-crack closure and is used to calculate the applied stress level at which the crack-tip stress field becomes effective in causing material damage during cyclic loading. Then, Elber's ΔK_{eff} range is calculated from the crack-opening stress, which is determined from the *K*-contact method [39]. The ΔK_{eff} range is shown in Equation 2.3 where S_{max} is the maximum stress, S_o is the crack-opening stress, c is the crack length, and F is the boundary-correction factor. The boundary-correction factor accounts for the effects on the configuration on stress-intensity factors. The boundary-correction factor is an equation that depends on a specimen's crack length and width. Equation 2.4 shows the boundary-correction factor equation for a C(T) specimen and Equation 2.5 shows the equation for a SEN(B) specimen. For C(T) and SEN(B) specimens, the nominal stress is given by *P/(WB)*.

$$\Delta K_{eff} = (S_{max} - S_o)\sqrt{\pi c}F \tag{2.3}$$

$$F_{C(T)}\left(\frac{c}{W}\right) = \frac{\left(2+\frac{c}{W}\right)\left[0.886+4.64\left(\frac{c}{W}\right)-13.32\left(\frac{c}{W}\right)^2+14.72\left(\frac{c}{W}\right)^3-5.6\left(\frac{c}{W}\right)^4\right]}{\left(1-\frac{c}{W}\right)^{\frac{3}{2}}} \tag{2.4}$$

$$F_{SEN(B)}\left(\frac{c}{W}\right) = -2.242 + 39.567\left(\frac{c}{W}\right) - 167.9\left(\frac{c}{W}\right)^2 + 335\left(\frac{c}{W}\right)^3 - 315.3\left(\frac{c}{W}\right)^4 + 112.82\left(\frac{c}{W}\right)^5 \tag{2.5}$$

In order to calculate ΔK_{eff}, it is necessary to determine the stress-intensity factor at which the crack tip opens, K_{op}. As seen in Figure 2.6 [36], ΔK_{eff} is the loading range

during which the crack is open. For low load ratio ($R = 0.1$) tests, the information provided by the BFS gage can be used to determine K_{op} from ASTM E-647. For high-R tests, however, the BFS gage is not sensitive enough to find a crack opening load. For these tests, a local strain gage, as described by Yamada [37], was sometimes used to find the crack opening loads for calculating ΔK_{eff} for each test. For ΔK, it is defined as the difference between the maximum and minimum applied K.

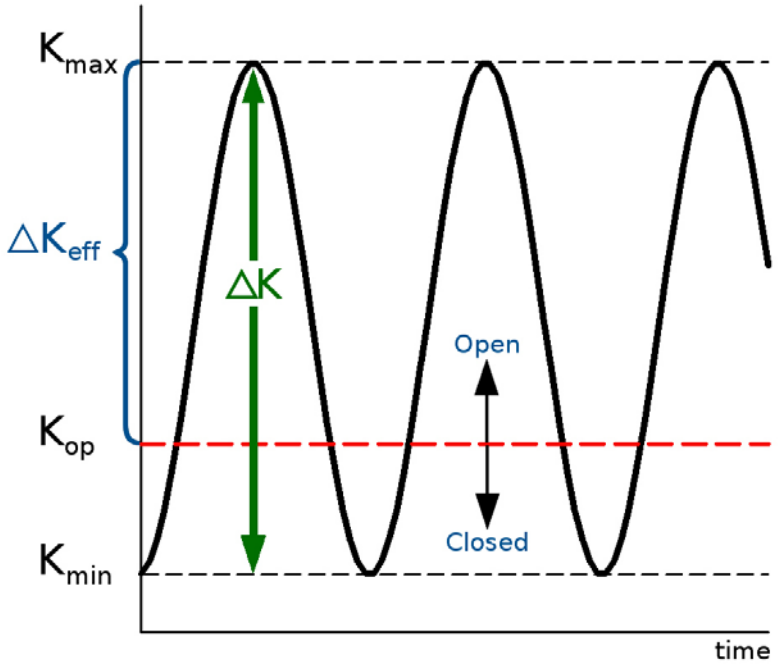

Figure 2.6 ΔK_{eff} is the stress-intensity factor ranging from K_{max} to K_{op}

For FASTRAN, fatigue-crack-growth-rate data must be generated over many orders-of-magnitude in rates from threshold to fracture for a wide range of load ratios from negative to positive ratios and must be in the form of ΔK against crack-growth-rate. These results are then used to establish the ΔK_{eff}-rate relation for the particular material, thickness, and testing environment. The crack-growth relation in FASTRAN, shown in Equation 2.6, is a multi-linear relation with terms to account for threshold and fracture,

where C_{1i} and C_{2i} are the coefficient and power for each linear segment, ΔK_o is the effective stress-intensity factor range threshold, K_{max} is the maximum applied stress-intensity factor, K_{Ie} is the elastic fracture toughness (which is, generally, a function of crack length, specimen width, and specimen type), p and q are constants selected to fit test data in either the threshold or fracture regimes. Whenever the applied K_{max} value reached K_{Ie}, then the rate would go to infinity and the specimen or component would fail. The multi-linear table-lookup is used instead of the sigmoidal form because many materials, especially aluminum alloys, show sharp changes in the crack-growth-rate curves at unique values of rates. For the 7050 alloy's testing purposes, threshold behavior was modeled with a multi-linear relation with $\Delta K_o = 0$ and $K_{Ie} = 50\ MPa\sqrt{m}$.

$$\frac{dc}{dN} = C_{1i}\left(\Delta K_{eff}\right)^{C_{2i}} \frac{\left[1-\left(\frac{\Delta K_o}{\Delta K_{eff}}\right)^{p}\right]}{\left[1-\left(\frac{K_{max}}{K_{Ie}}\right)^{q}\right]} \tag{2.6}$$

A key trait of the model is its ability to simulate three-dimensional stress-state effects, like plane-strain or plane-stress conditions, around the crack front by using plastic-constraint factors for tension (α) and compression (β). In predicting crack-growth under spectrum loading, it is essential to choose the proper constraint factors.

In FASTRAN, the applied cyclic loading can be constant- or variable-amplitude and tensile or compressive loads can be applied. The program includes several standardized flight-load spectra and the user can also input spectrum loads as either a list of stress points, flight-by-flight sequence, or a flight schedule. FASTRAN uses a damage rule that does not require a rainflow counting of the loading sequences. The code uses what is called rainflow-on-the-fly damage rule because crack-tip damage occurs due to the current loading and the loading history, and does not depend upon future loading. The program uses the crack-closure concept to account for load-interaction effects.

FASTRAN contains twenty-two predefined crack configurations and the user can define two other types of crack configurations. The crack-opening stresses, as a function of load history and crack length, are calculated from the model and the effective stress-intensity factor range, used to correlate fatigue-crack-growth-rates, may be either elastic or modified for plastic yielding at the crack tip.

CHAPTER III

CONSTANT-AMPLITUDE LOADING

Standard compact specimens were tested to generate the ΔK against rate data over a range in load ratios of 0.1, 0.7, and 0.9 from threshold to near fracture. These data were used to generate the crack-closure based ΔK_{eff}-rate curve that is used to make fatigue-crack-growth predictions on C(T) specimens and fatigue-life predictions on SEN(B) specimens subjected to a wide range of loading conditions.

3.1 Compact C(T) Specimens

Figure 3.1 shows the ΔK-rate data generated on a range of load ratios using the CPLR test method in the low rate regime and constant-amplitude loading at higher rates. In addition, two K_{max} tests were conducted to generate data at very high-R [30]. The crack-closure model FASTRAN [6,7,40] was then used to find a constraint factor (α) that would correlate the ΔK-rate data into a tight band on the ΔK_{eff} plot, as shown in Figure 3.2. Surprisingly, a very low constraint factor of $\alpha = 1.3$ was required. The data correlated very well and even collapsed onto a unique curve in the near-threshold regime.

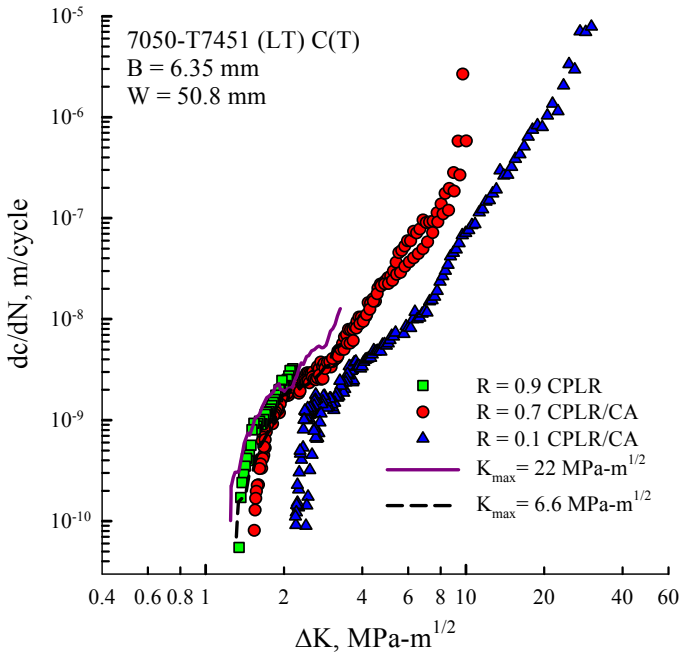

Figure 3.1 Fatigue-crack-growth-rate data on the 7050-T7451 aluminum alloy

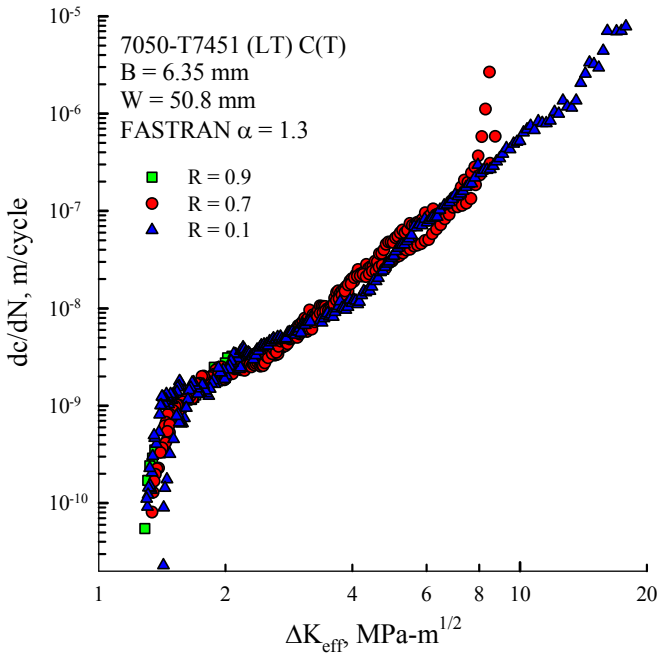

Figure 3.2 Correlation of fatigue-crack-growth-rate data using FASTRAN

During the C(T) specimen testing, crack lengths were monitored using compliance data from BFS gage. Compliance data from the closure-free portion of the load cycle is used to determine crack length, enabling the tests to be automated and computer controlled. Load-against-strain data can also be used to measure crack-closure events. A typical load against BFS record during a CPLR (threshold) test is presented in Figure 3.3 for $R = 0.1$. The compliance is constant at high loads, which appears as a linear section in the upper right portion in Figure 3.3. As the load decreases, crack surfaces contact and produce a change in compliance. The reduced-strain, or displacement, method was developed to improve detection of these subtle compliance changes [41]. The reduced strain, $\Delta\varepsilon$, is the deviation from closure-free compliance behavior, and this behavior becomes a vertical line on these plots, making compliance deviations easier to detect from load-against-reduced strain plots. Using the reduced-strain method, considerable deviation is observed at low loads ($P/P_{max} < 0.7$) in Figure 3.3. The very high crack-opening load was assumed to be caused by plasticity and roughness-induced crack-surface contact, but this method does not provide information about the location of crack-face contact since this method relies on changes in compliance to determine closure (or crack-opening) levels.

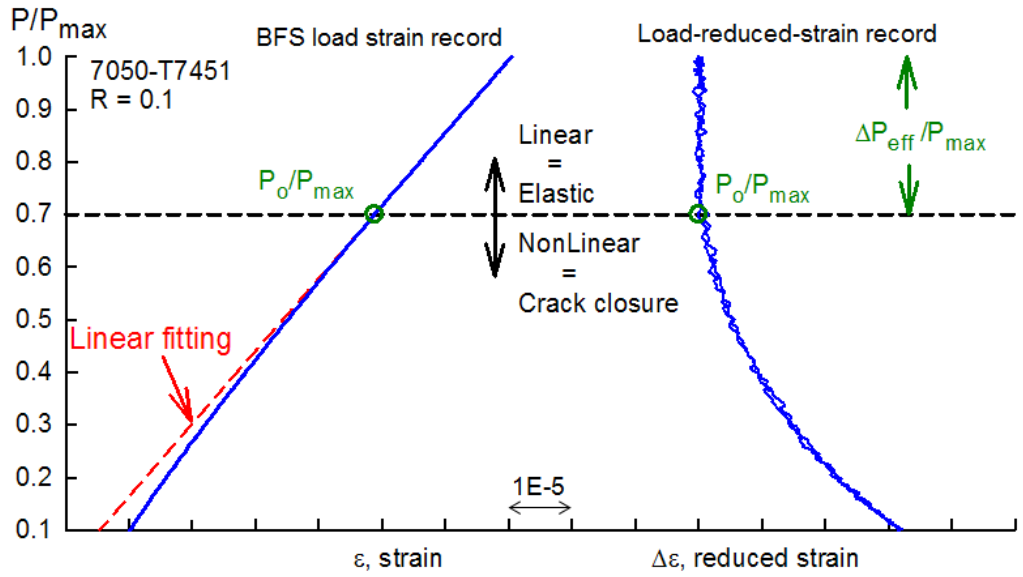

Figure 3.3 Load-against-backface-strain on a C(T) specimen tested at low-*R* conditions and Elber's method of determining crack-opening loads

Recently, Yamada and Newman [42,43] have used local strain gages mounted on one side of C(T) specimens to measure crack-opening loads. Figure 3.4 demonstrates how local strain and BFS gages are mounted on C(T) specimens. In measuring load-strain records, either from BFS or local strain gages, it is extremely important that nonlinearities, such as that due to out-of-plane bending or other causes, are not present in the measured data. Beveling the pin-holes in the C(T) specimens also reduced any out-of-plane bending, which helped in maintaining linearity. So, a notch C(T) specimen was tested without a fatigue crack to verify the linearity of the local load-strain records. Figure 3.5 shows load-against-reduced strain records for a notched and cracked specimen at low- and high-R conditions. The records with only a notch were very linear, while the records with a fatigue crack show the typical crack-closure behavior. Where the nonlinear curve meets the upper linear portion is assumed to be the crack-opening load [41]. These results show that even the $R = 0.7$ near-threshold test develops crack closure,

which was not anticipated. The literature has suggested that high-*R* tests are crack-closure free, but the works of Yamada and Newman [42,43] has shown that high-*R* and K_{max} tests on a variety of materials develops significant crack closure in the threshold regime.

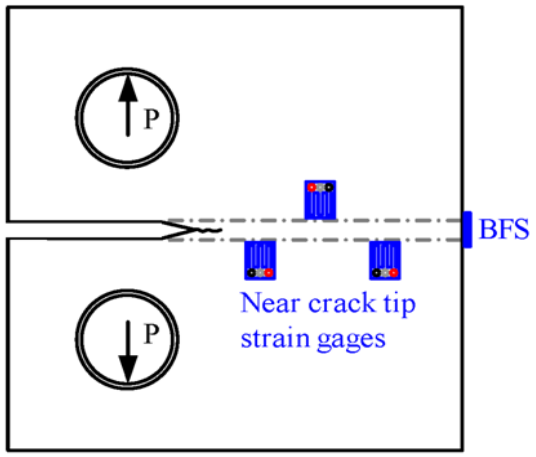

Figure 3.4 C(T) specimen with backface strain (BFS) and local strain gages

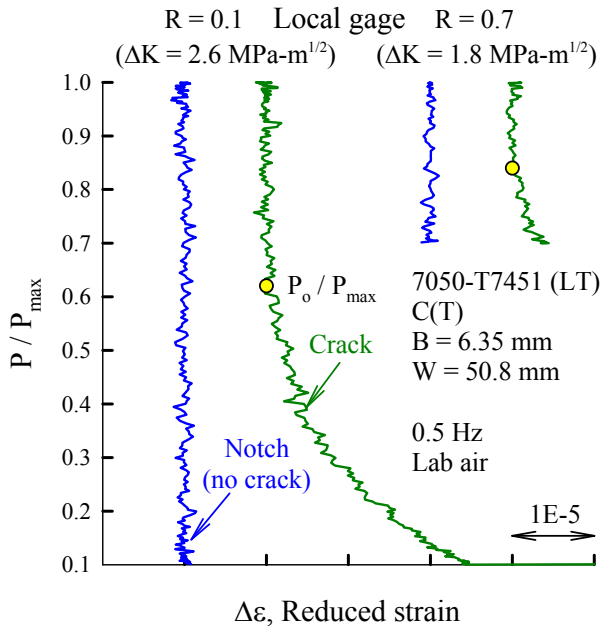

Figure 3.5 Crack-opening loads on typical low- and high-*R* test cases

Using measured crack-opening ratios [30], the ΔK_{eff} values were determined and compared with the ΔK-rate data generated on constant R and two K_{max} tests in Figure 3.6. The ΔK_{eff} data fell at very low stress-intensity values in the near-threshold regime due to the very high crack-opening-load ratios, but fell slightly to the upper bound of the $R = 0.7$ results in the mid- and upper-rate regions. This implies that in the mid- to upper-rate regions, only a small amount of crack closure is occurring at $R = 0.7$. This was anticipated due to previous research. The lines in Figure 3.6 show the selected ΔK_{eff}-rate curves, upper and lower bound rates. The discrepancy is due to the fact that FASTRAN is a plasticity-induced crack-closure (PICC) model and roughness- and/or fretting-debris play a dominant role in the threshold regime for the 7050 alloy. These ΔK_{eff}-rate values are listed in Table 3.1 [30], where the upper bound rates were obtained from local strain gage readings and the lower bound rates were from BFS gage readings.

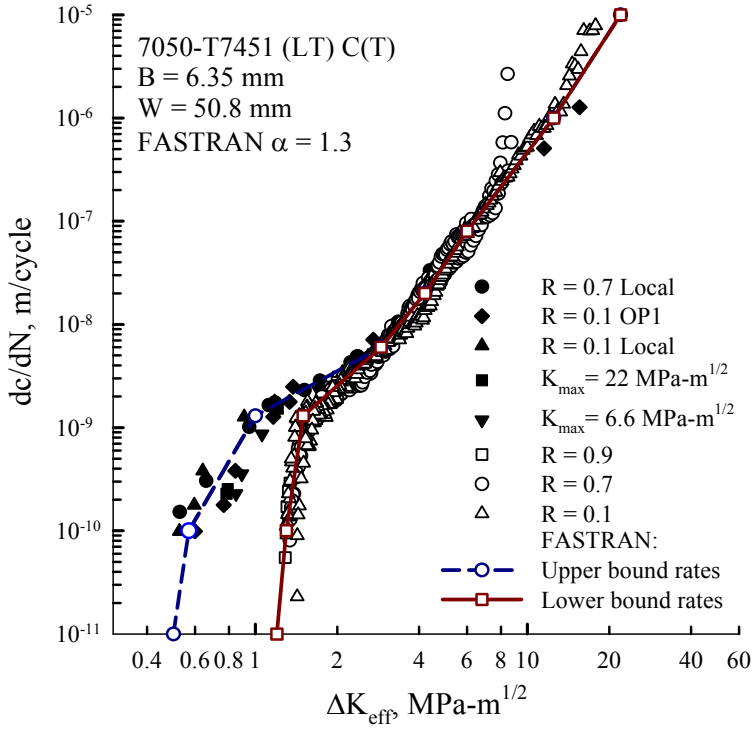

Figure 3.6 Fatigue-crack-growth-rate data using measured crack-opening loads

Table 3.1 Effective stress-intensity factor range against rate relations for 7050-T7451 aluminum alloy

Upper bound (ΔK_{eff}, MPa$\sqrt{m}$)	Lower bound (ΔK_{eff}, MPa$\sqrt{m}$)	Rate (dc/dN, m/cycle)
0.5	1.2	1.0e-11
0.57	1.3	1.0e-10
1.0	1.5	1.3e-10
2.9	2.9	6.0e-09
4.2	4.2	2.0e-08
6.0	6.0	8.0e-08
12.5	12.5	1.0e-06
22.0	22.0	1.0e-05
$\alpha = 1.3$	$\alpha = 1.3$	All rates
$K_{Ie} = 50$ MPa$\sqrt{m}$	$K_{Ie} = 50$ MPa$\sqrt{m}$	$\sigma_o = 498$ MPa

3.2 Single-Edge-Notch Bend SEN(B) Specimens

Barter et al [28] has done an extensive study on the distribution of inclusion particle sizes for the 7050 aluminum alloy. Figure 3.7 shows the cumulative distribution function for the inclusion-particle depths on high stress-concentration ($K_T = 3$) coupons. The median particle depth was about 12 μm, while the 10 and 90 percentile depths were 4 and 30 μm. The initial discontinuity was assumed to be a semi-circular surface crack ($a_i = c_i = 12\ \mu m$) located at the center of the edge-notch. Two- and three-dimensional stress-intensity factor solutions were developed for the SEN(B) specimen and incorporated into the FASTRAN code [36]. Walker and Barter [29] have also shown that the upper bound curve in Figure 3.6 agreed well with small-crack data generated on the 7050 alloy. So, the fatigue behavior of the notched specimens may be predicted using small-crack theory.

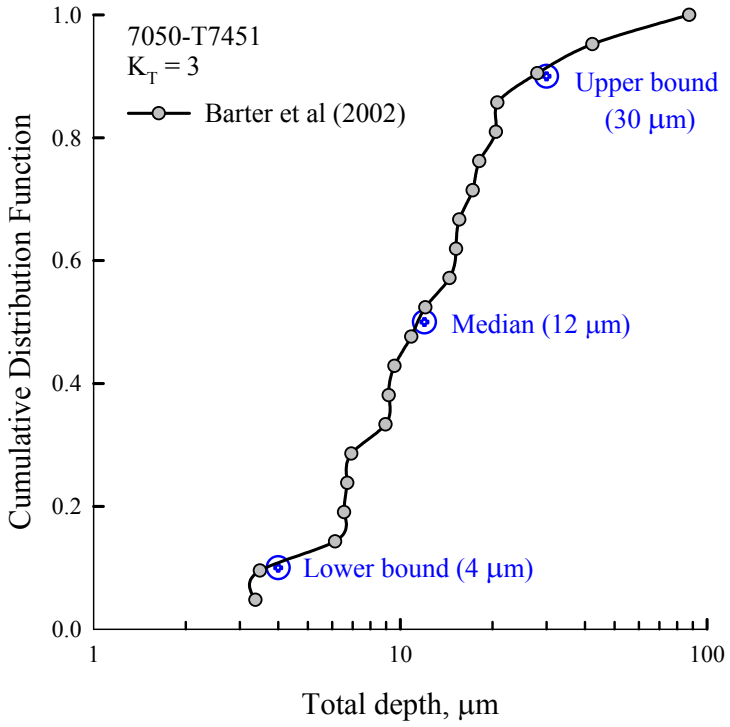

Figure 3.7 Distribution of discontinuities (inclusion sizes) in high K_T specimens made of 7050-T7451 aluminum alloy

Figure 3.8 shows the stress life (*S-N*) data on the SEN(B) specimens tested at $R = 0.1$. A nominal stress, $P_{max}/(WB)$, was plotted against the fatigue life, N_f. The curves shown are the FASTRAN predictions on fatigue lives using the lower and upper bound curves, respectively. For the low-cycle fatigue (LCF) region, both curves predicted essentially the same fatigue lives that agreed well with the test data. At the lower applied stress levels, the lower-bound curve slightly over predicted the fatigue lives, while the upper bound curve was highly conservative. This is shown by the dashed lines in Figure 3.8.

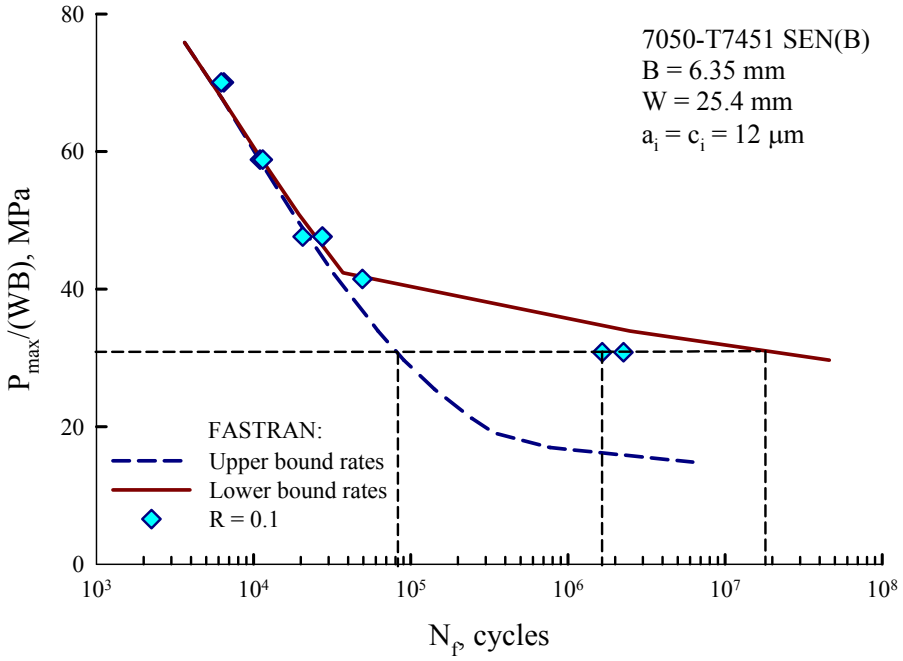

Figure 3.8 Fatigue life behavior under constant-amplitude loading

Figure 3.9 shows how the initial discontinuity size influenced the predicted fatigue lives. For LCF conditions, the initial flaw size had some influence on the fatigue lives, but for high-cycle fatigue (HCF) conditions, the initial flaw size had a very large

influence on the fatigue lives, as expected. Since the results using the median flaw size agreed well with the constant-amplitude test data, the median flaw size will be used for all spectrum load cases.

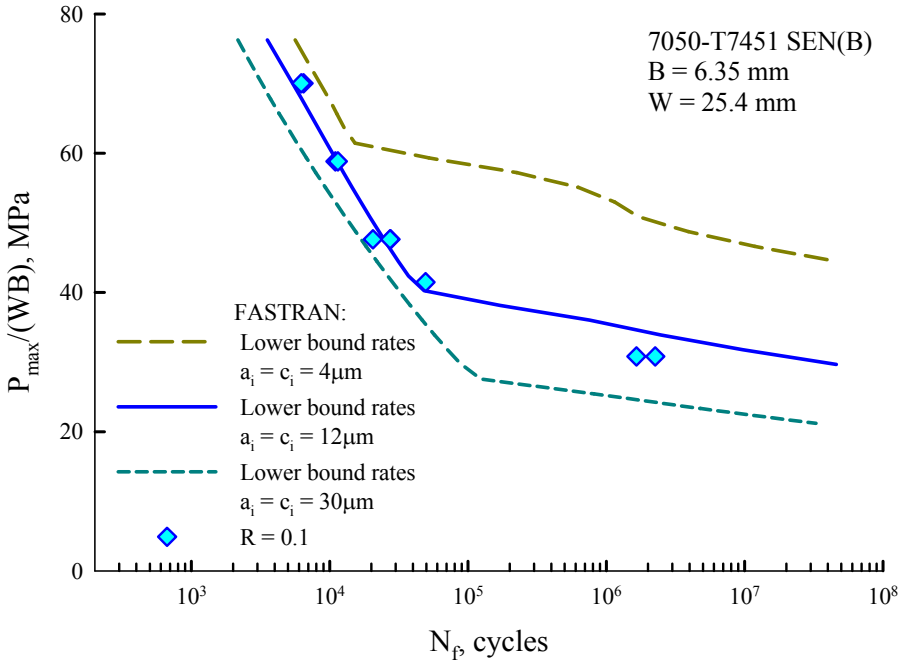

Figure 3.9 Fatigue life behavior under constant-amplitude loading for various initial inclusion sizes

CHAPTER IV

SINGLE-SPIKE OVERLOADS

Several repeated spike overload tests were conducted on three C(T) specimens to determine the effects on crack-growth delay. Two specimens were in the longitudinal (LT) direction and one was in the transverse (TL) direction. These tests are useful in establishing and/or validating α that is used in the crack-closure model. In addition, the BFS record was used to investigate crack-closure behavior before and after the single-spike overload. Some typical results are shown in Figure 4.1, after the second overload on a C(T) specimen at a crack length of about 23 mm. This figure shows the normalized load against reduced strain (volts) for the loading and unloading record. The large tail swing below P/P_{max} of 0.8 is believed to indicate crack closure. The crack-monitoring system [44] recorded the 1% and 2% (*OP1* and *OP2*) compliance offset values per ASTM E-647 [45]. Using Elber's method [39], the crack-opening value is about 0.8. This is significantly higher than either the *OP1* or *OP2* values. A 0% offset value (*OP0*) can be estimated from *OP1* and *OP2*, as shown, which is closer to the actual crack-opening value of 0.8, but *OP0* is still about 10% lower than 0.8. The ASTM E-647 method was not developed for variable-amplitude loading, so further study is needed to establish a more reliable method.

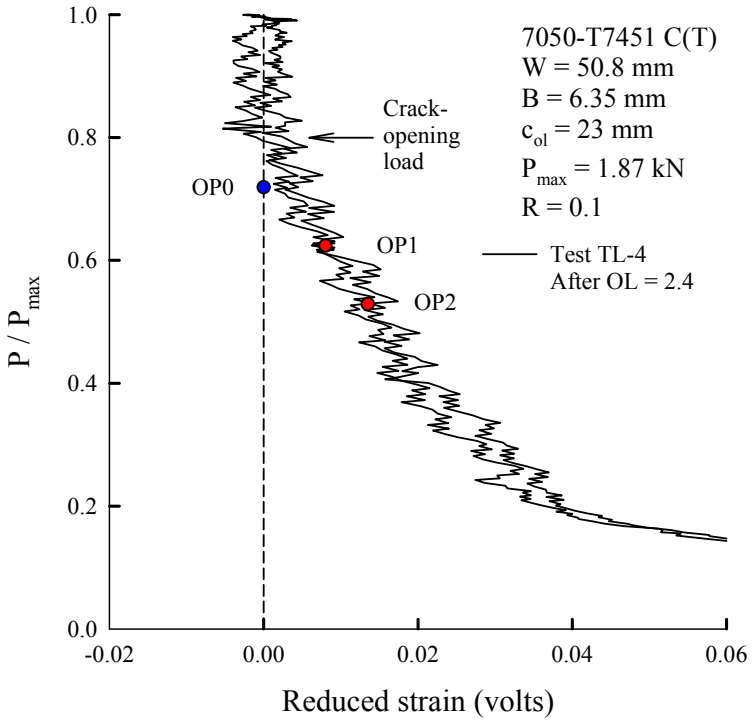

Figure 4.1 Load-against-reduced strain after 2.4 overload

Figure 4.2 shows the crack length against cycles for the repeated 2.6 spike overload test and indicates a significant retardation after the application of the 2.6 overload. After the second overload and 8 million cycles, the specimen was pulled to failure to determine some fracture toughness information. FASTRAN predicted that the crack would become dormant after the first overload but this was not seen in the test. The test showed the crack would grow through the overload plastic zone. This was also noticed in the next spike overload test. For the second specimen, (LT-14), the first spike overload was 2.6 and the second one was 2.0. Even though the overload of 2.0 was hardly noticed during the test, the crack was shown to grow through the overload plastic zones. However, FASTRAN still predicted that the crack would not grow after the first overload as seen in Figure 4.3.

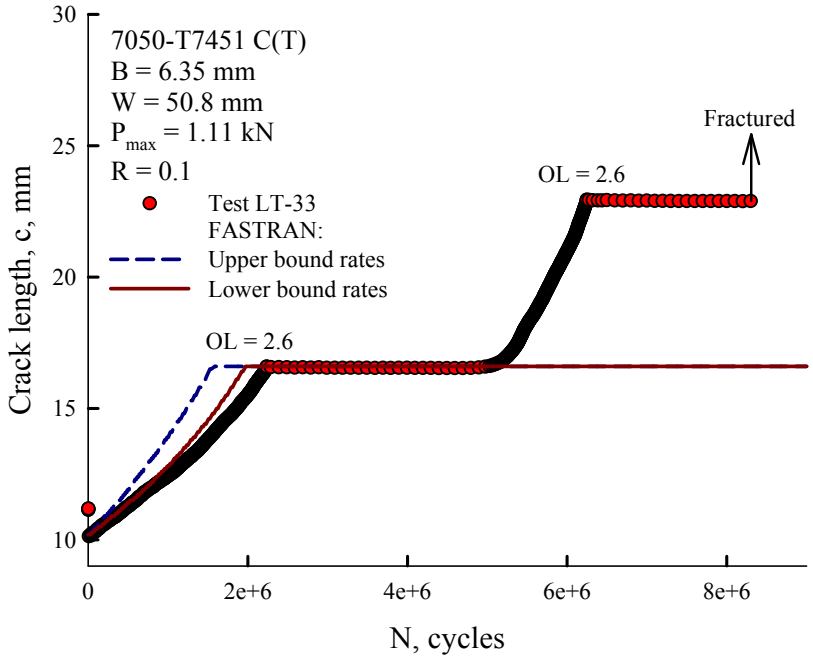

Figure 4.2 Crack-length-against-cycles for repeated 2.6 spike overloads

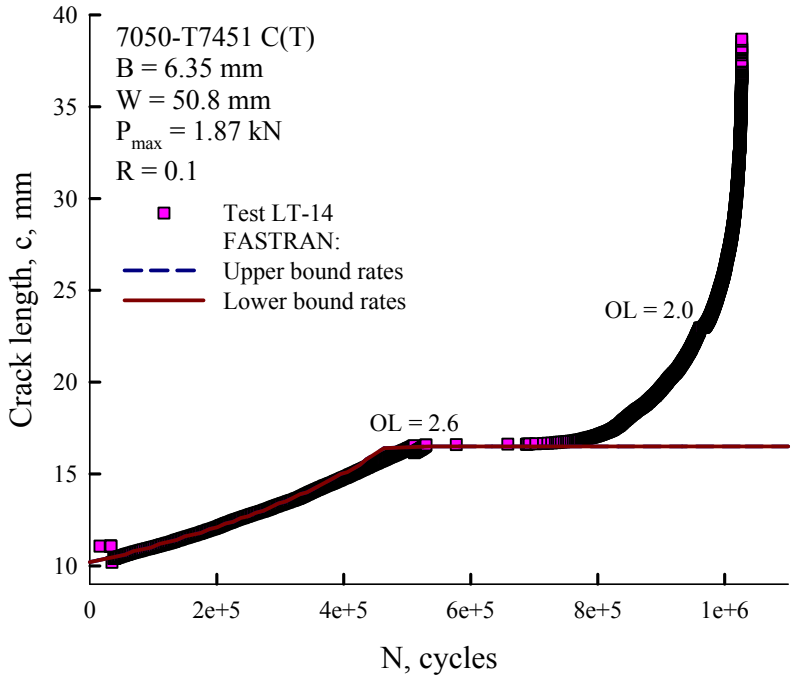

Figure 4.3 Crack-length-against-cycles for 2.6 and 2.0 spike overloads

After some consideration, it was believed that an overload factor of 2.6 was too severe for FASTRAN to predict. The crack-closure model was designed to grow a crack straight through the overload plastic zone, as shown in Figure 4.4. However, because of the very rough fatigue-crack surface and slip-band formation at the crack front during the overload, the crack may grow around the overload plastic zone as shown in Figure 4.4. Crack path changes have been observed by White et al [46] on the 7050-T7451 alloy for periodic under loads and Hudson [47] on 2024-T3 after a two-level (2:1 applied stress level) block loading test.

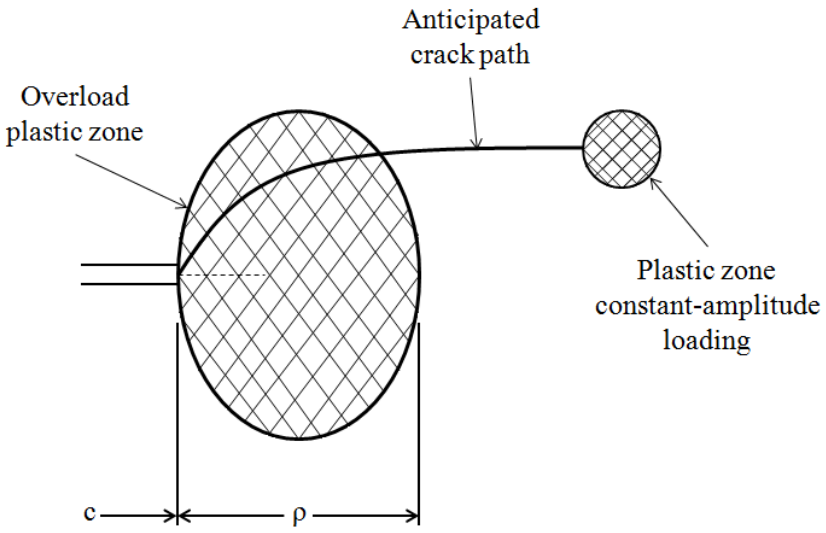

Figure 4.4 Suspected crack path after high overload

A third test was performed on a TL C(T) specimen with repeated 2.4 spike overloads. As before, FASTRAN predicted the crack would become dormant after the first overload but this was true when using the lower bound rates. When evaluating the test using the upper bound rates, FASTRAN was able to predict the spike overloads as shown in Figure 4.5. FASTRAN was only off by a factor of two in life for each overload.

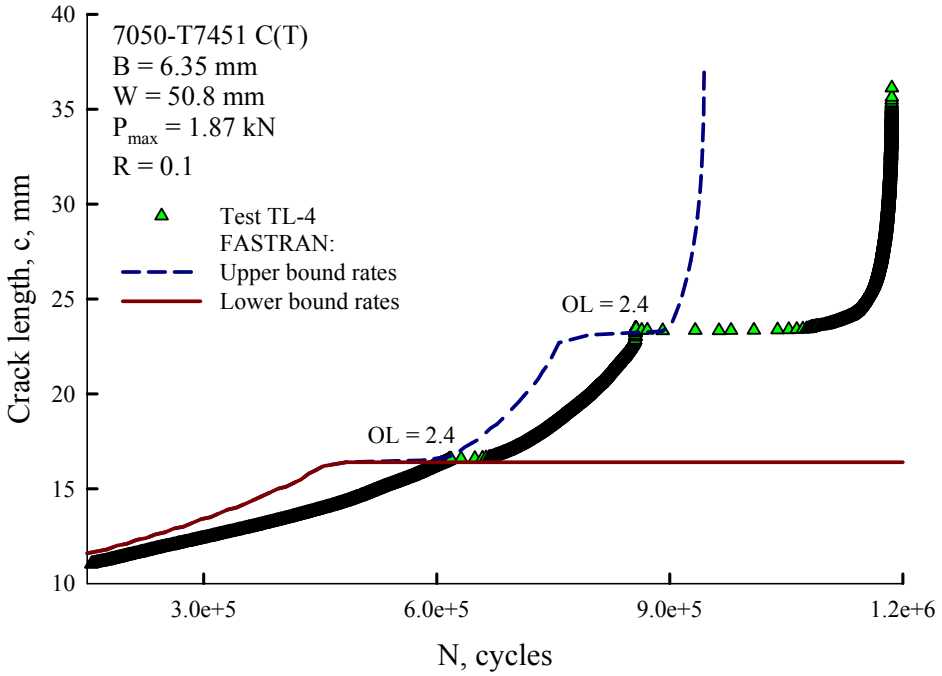

Figure 4.5 Crack-length-against-cycles for repeated 2.4 spike overloads

CHAPTER V

MINI-FALSTAFF+ SPECTRUM LOADING

Mini-Falstaff+ is a European standard load sequence for fighter aircraft wing structures. The original Mini-Falstaff sequence has 9,006 cycles, which is equivalent to 200 flights [31,32]. The limitations in C(T) specimens made it impossible to use the Mini-Falstaff loading because of the compressive loads. Instead, a similar spectrum was created to verify the effectiveness of FASTRAN to predict crack-growth under a similar spectrum loading. The spectrum, Mini-Falstaff+, was derived from the Mini-Falstaff spectrum by adding a mean load, as shown in Equation 5.1.

$$Mini\text{-}Falstaff+ = \frac{Mini\text{-}Falstaff+0.3667}{1.3667} \tag{5.1}$$

This made sure that the maximum normalized load in the sequence is unity and the minimum normalized load is one-tenth, removing the compressive loads entirely. Some of the Mini-Falstaff+ sequences are shown in Figure 5.1. The Mini-Falstaff+ spectrum were applied to the specimens at a constant load rate, which produced an average frequency of about 3 Hz or 50 minutes per 9,006 cycles. Before testing the specimens, correlation data files had to be made for each test on the C(T) and SEN(B) specimens. These correlation files are used by the crack monitoring system [44] so that each peak load is reached during each flight sequence. Generally, three flights, or passes, are needed to calibrate the correlation files so that the crack monitoring system [44] will be able to reach the peak loads throughout the test.

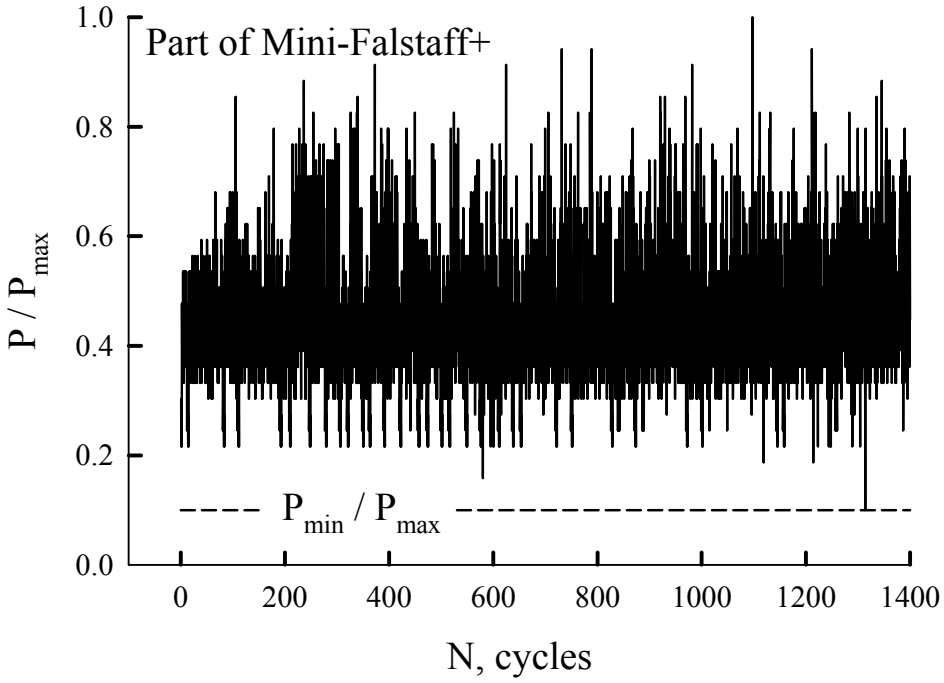

Figure 5.1 Part of Mini-Falstaff+ load spectrum

5.1 Compact C(T) Specimens

Figure 5.2 shows crack-length-against-cycles on 3 tests conducted on C(T) specimens in the LT orientation under the Mini-Falstaff+ spectrum loading. These tests were conducted at a maximum load (P_{max}) of 4.45 kN. Test LT-26 used CPCA loading and Test LT-28 used tensile precracking to grow the crack from the initial EDM notch length to about 12.5 mm, and then the spectrum loading was applied. During the test on Specimen LT-26, the last 25% of the data was lost due to system failure. Fortunately, the failure crack length and cycle were recorded visually and this data point is in Figure 5.2. The test results were basically independent of how the crack was initiated from the crack-starter notch. In test LT-27, the spectrum loading was applied from the start with no fatigue precracking. FASTRAN slightly over predicted (8% to 16%) the crack-length-against-cycle results from the tests.

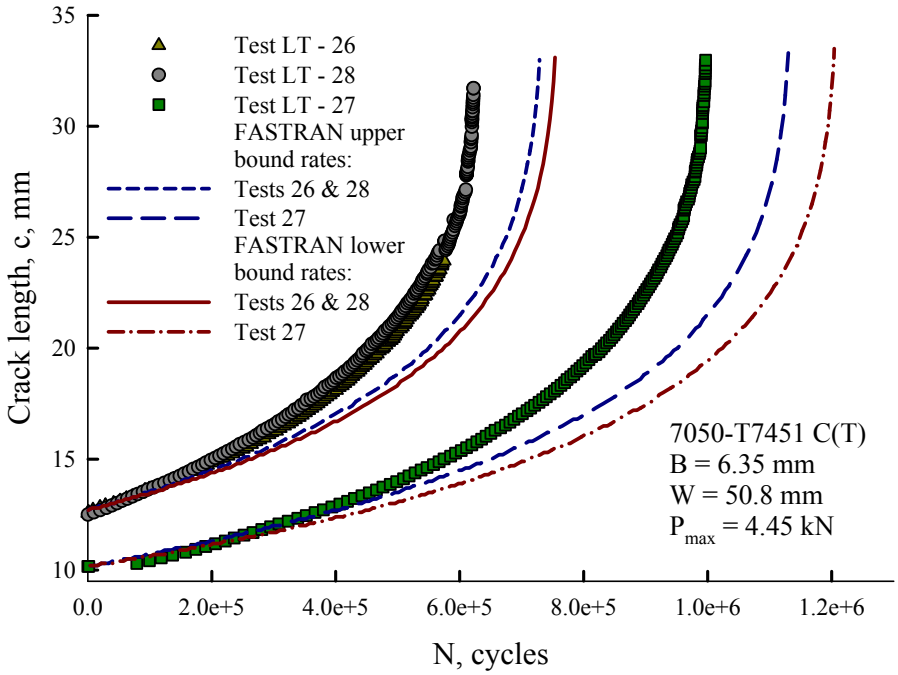

Figure 5.2 Crack-length-against-cycles for C(T) specimens under Mini-Falstaff+ loading

5.2 Single-Edge-Notch Bend SEN(B) Specimens

A large number of SEN(B) specimens were tested under the Mini-Falstaff+ load sequence as shown in Figure 5.3. A nominal stress based on the maximum load applied in the spectrum was plotted against the fatigue life. One test was terminated at 10^7 cycles. The lower bound curve agreed well with the test data over the complete range of maximum loads applied in the spectrum. Whereas, the predicted lives from the upper bound curve were conservative for all maximum loads tested.

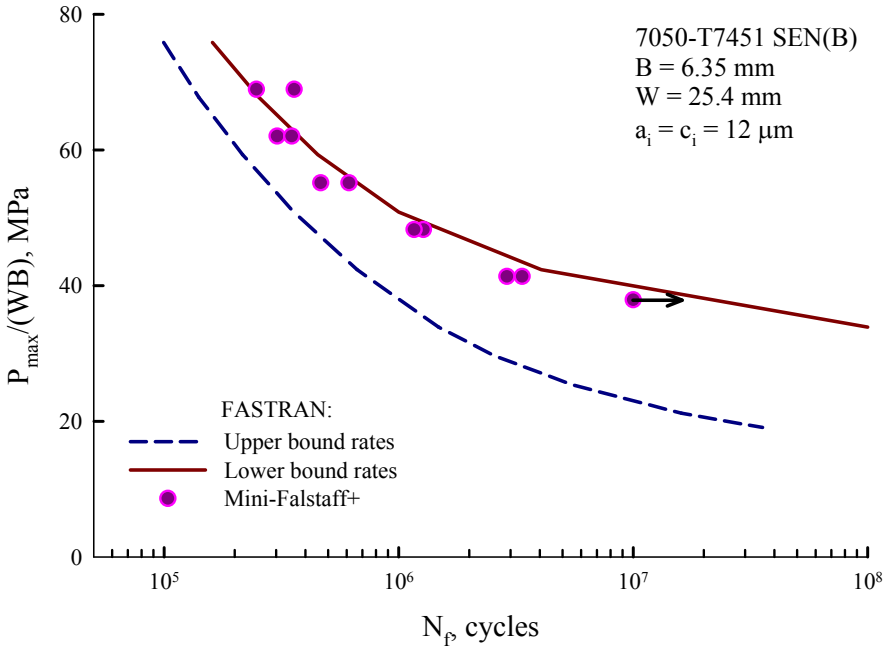

Figure 5.3 Fatigue life behavior under Mini-Falstaff+ loading

CHAPTER VI

MINI-TWIST+ SPECTRUM LOADING

Mini-TWIST [34] is a European standard gust load sequence for transport aircraft wings. Load spectra pertaining to wing root stresses were obtained from several transport aircraft types. The standardized flight loading sequence was taken as the average of the different load spectra. Mini-TWIST represents a load sequence for a block of 4,000 flights that are composed of 10 distinct flight types. Stress levels in each flight were normalized by the *1-g* mean stress in flight S_{mf} during cruise conditions. The highest peak stress $S_{max} = 2.6S_{mf}$ occurs only once in the total sequence. The lowest trough (or minimum stress) is $S_{min} = -0.6S_{mf}$.

A mean load was added to the original Mini-TWIST load sequence to maintain a global *R* ratio of 0.1, as shown in Figure 6.1 for Mini-TWIST+ Level 1. This figure shows part of the severest flight in the Mini-TWIST spectrum. Mini-TWIST+ Level 3 was obtained by truncating load levels 1 and 2 to level 3, as shown by the upper dashed line.

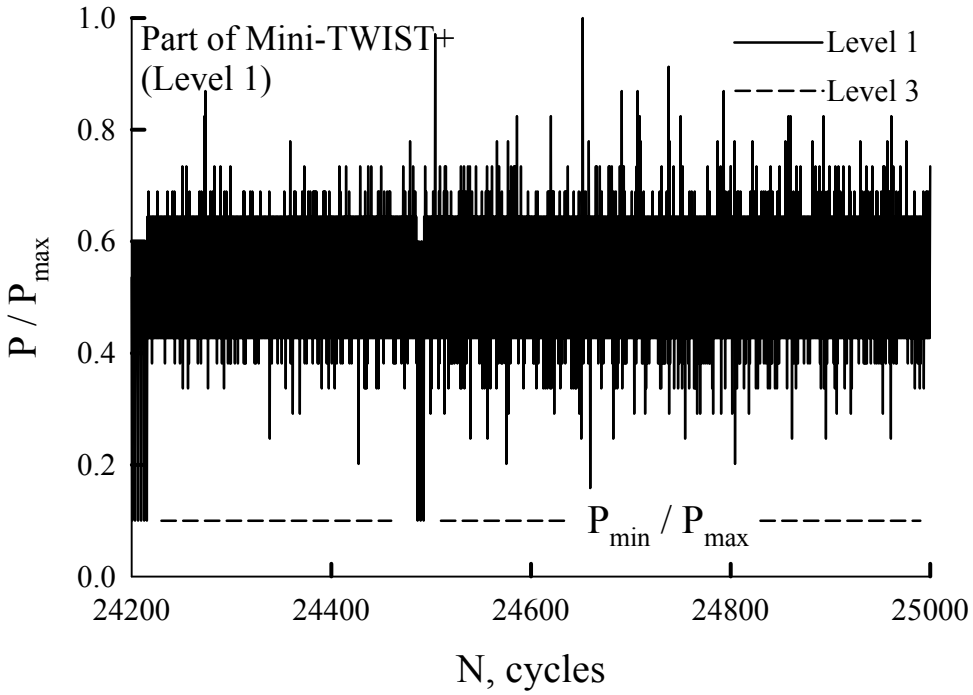

Figure 6.1 Part of Mini-TWIST+ load spectrum

The fatigue tests and life-predictions made on specimens subjected to the Mini-TWIST+ spectrum loading are shown in Figures 6.2 and 6.3. Results using the full Mini-TWIST+ Level 1 spectrum are shown in Figure 6.2, and it shows that the lower bound curve over predicted the fatigue lives by a factor of 3 using the 12 μm initial flaw. The test data fell between the predicted lives from the lower and upper bound curves, whereas the predicted results on Mini-TWIST+ Level 3 spectrum agreed well with the test data. Figure 6.4 shows the data from the Mini-TWIST+ Levels 1 and 3 tests plotted against the lower bound rates. All of the data fell on the lower-bound Level 3 curve. It is suspected that the high loading in the severe flight Level 1 are causing more crack-growth delay in the model than Level 3 loading. These results are similar to the single-spike overload results, which caused the predicted crack to become dormant. Once more, the rough crack surfaces may promote more crack-front meandering around overload plastic zones,

while FASTRAN model was forcing the crack to cut straight through the overload plastic zones. As stated before, further study is needed to help resolve these issues with severe overloading during variable-amplitude loading.

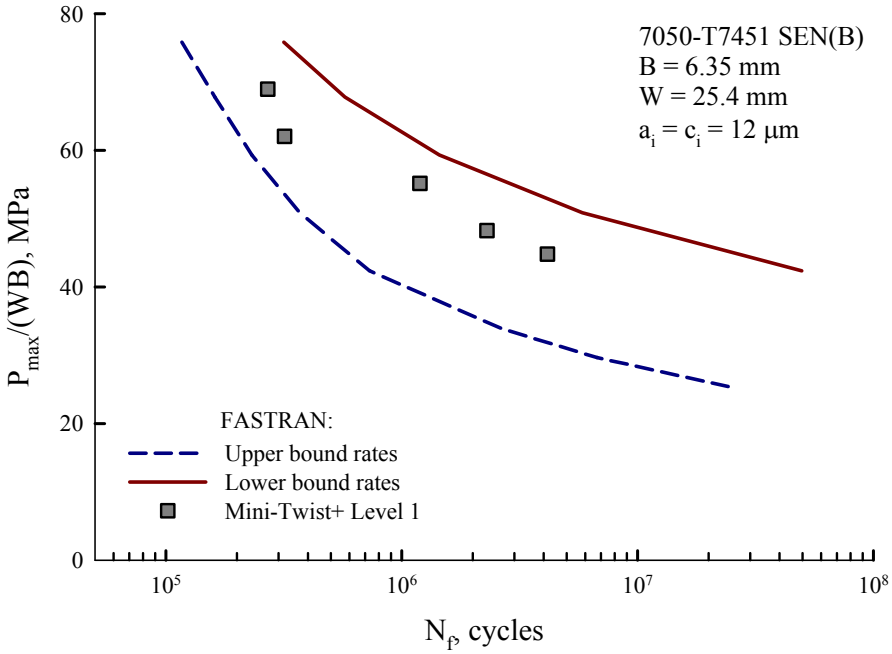

Figure 6.2 Fatigue life behavior under Mini-TWIST+ Level 1 loading

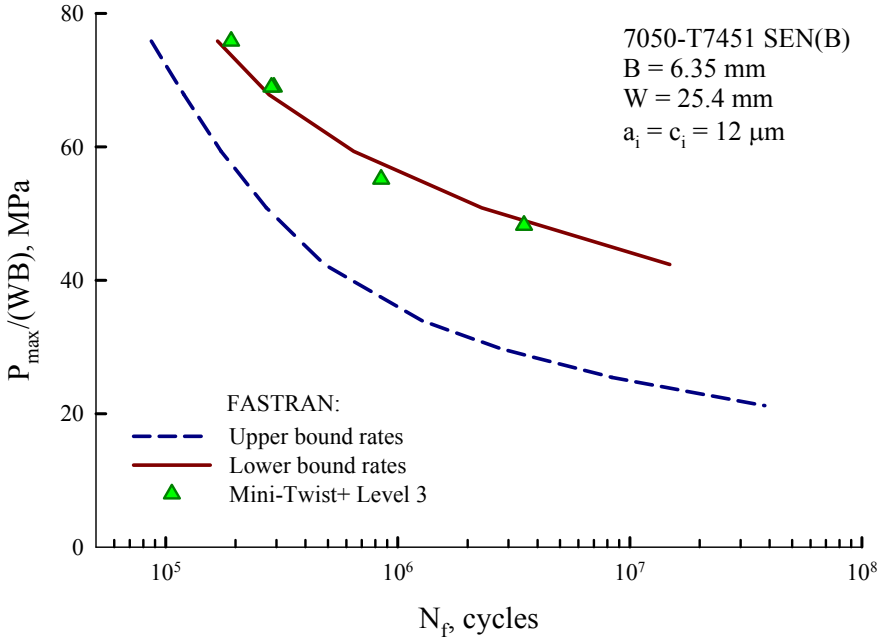

Figure 6.3 Fatigue life behavior under Mini-TWIST+ Level 3 loading

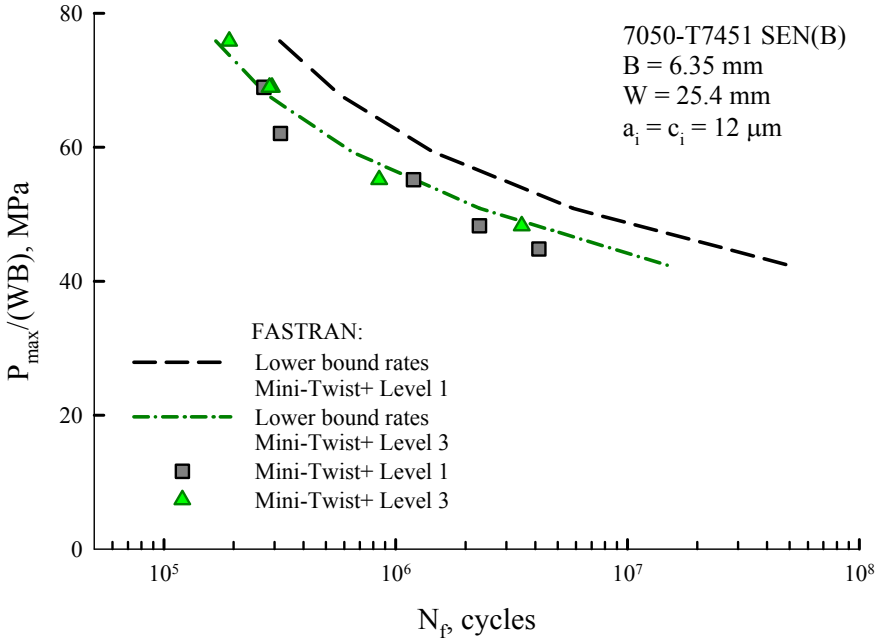

Figure 6.4 Fatigue life comparison for Mini-TWIST+ Levels 1 and 3 with lower-bound rates

CHAPTER VII

CLOSING REMARKS

In summary, this work described the efforts to test and characterize the 7050-T7451 aluminum alloy. Testing performed included fatigue-crack-growth testing, single-spike overloads, and a simulated aircraft spectrum loading on C(T) specimens. Fatigue tests were also conducted on SEN(B) specimens over a wide range in loading conditions, including constant-amplitude and three aircraft spectra loading. The two European standard spectra were modified to have only tension-tension loading. All specimens were machined from a single forged block of 7050-T7451, however, no residual stresses were measured in both the SEN(B) and C(T) specimens.

7.1 Conclusions

The purpose of this thesis was to evaluate two different ΔK_{eff} curves for making crack-growth and fatigue-life predictions. These two curves came from C(T) tests previously conducted on the same batch of 7050 aluminum alloy. Small-crack theory was used to make fatigue-life predictions using inclusion-particle sizes from the literature. Fatigue predictions on the SEN(B) specimens agreed fairly well (±30%) using a 12-micrometer initial flaw located at the semi-circular-edge-notch under all loading conditions, except the model was un-conservative (factor of 3) on the Mini-TWIST+ Level 1 spectrum. For the C(T) specimens subjected to single-spike overloads, the life-prediction code produced much more retardation than observed in the tests, except for the repeated 2.4 spike overloads using the upper bound rates. The predicted crack-length-

against-cycles under Mini-Falstaff+ spectrum loading were only 15% longer than the tests. The discrepancy under the single-spike overloads and Mini-TWIST+ Level 1 was suspected to be caused by using a low constraint factor and/or crack paths meandering around overload plastic zones. Ideally, a roughness-induced crack-closure model, in addition to the plasticity model, would be needed to obtain more reasonable results.

7.2 Future Work

Even though FASTRAN has demonstrated the ability to simulate the behavior of most constant-amplitude and some variable-amplitude and spike overload tests, it is essential to recognize that not all engineering structures experience such simplified cyclic loads in application. The ability to accurately and consistently predict the fatigue behavior of specimens exposed to standard spectrum of cyclic loads is limited to only a few spectra and materials. This is also true for single-spike overload tests. Therefore, it is imperative that this work be continued with investigations into spectrum loading sequences and spike overloads.

In order to better understand the effects of spectrum loading and spike overloads, it is important to clearly understand the behavior of a given material in the threshold regime. Currently, this understanding is limited by the lack of information on the effect that debris has on the growth of cracks in metals. FASTRAN needs to be modified in order to account for the added complexity of surface debris and crack-surface roughness. Materials that often produce rough fracture surfaces, like 7050 aluminum alloy, are an excellent place to start the study of crack-growth behavior not governed by plasticity only.

REFERENCES

[1] Elber, W., "Fatigue Crack Closure under Cyclic Tension," *Engineering Fracture Mechanics*, Vol. 2, 1970, pp. 37-45.

[2] Elber, W., "The Significance of Fatigue Crack Closure," *ASTM STP 486*, American Society for Testing and Materials, Philadelphia, PA, 1971, pp. 230-242.

[3] Schijive, J., "Fatigue Crack Closure Observations and Technical Significance," *ASTM STP 982*, American Society for Testing and Materials, Philadelphia, PA, 1988, pp. 5-34.

[4] NASGRO Reference Manual (version 4.02), NASA Johnson Space Center and Southwest Research Institute, 2002.

[5] AFGROW Reference Manual (version 4.0), AFRL/VASM, Wright-Patterson Air Force Base, Ohio, 2003.

[6] Newman, J. C., Jr., "FASTRAN II - A Fatigue Crack-growth Structural Analysis Program," *NASA TM 104159*, 1992.

[7] Newman, J. C., Jr., "A Crack-Closure Model for Predicting Fatigue Crack-growth under Aircraft Spectrum Loading," *ASTM STP 748*, American Society for Testing and Materials, Philadelphia, PA, 1981, pp. 53-84.

[8] de Koning, A. U., ten Hoeve, H. and Henriksen, T. K., "Description of Crack-growth using the Strip-Yield Model for Computation of Crack Opening Loads, Crack Tip Stretch, and Strain Rates," *ASTM STP 1343*, American Society for Testing and Materials, West Conshohocken, PA, 1999, pp.459-474.

[9] Pearson, S., "Initiation of Fatigue Cracks in Commercial Aluminum Alloys and Subsequent Propagation of Very Short Cracks," *Engineering Fracture Mechanics*, Vol. 7, 1975, pp. 235-247.

[10] Kitagawa, H. and Takahashi, S., "Applicability of Fracture Mechanics to Very Small Cracks or the Behavior in the Early Stages," Proc. Second International Conference on Mechanical Behavior of Materials, Boston, MA, 1976, pp. 627-631.

[11] Zocher, H., ed., "Behavior of Short Cracks in Airframe Components," *AGARD CP-328*, 1983.

[12] Ritchie, R. O. and Lankford, J., eds., "Small Fatigue Cracks," The Metallurgical Society, Inc., Warrendale, PA, 1986.

[13] Miller, K. J. and de los Rios, E. R., eds., "The Behavior of Short Fatigue Cracks," European Group on Fracture, Publication No. 1, 1986.

[14] Newman, J. C., Jr. and Edwards, P. R., "Short-Crack-growth Behavior in an Aluminum Alloy - an AGARD Cooperative Test Programme," *AGARD R-732*, 1988.

[15] Edwards, P. R. and Newman, J. C., Jr., eds., "Short-Crack-growth Behavior in Various Aircraft Materials," *AGARD R-767*, 1990.

[16] Newman, J. C., Jr., Wu, X. R., Venneri, S. and Li, C., "Small-Crack Effects in High-Strength Aluminum Alloys," *NASA RP-1309*, 1994.

[17] Newman, J. C., Jr., Swain, M. H. and Phillips, E. P., "An Assessmsent of the Small-Crack Effect for 2024-T3 Aluminum Alloy," Small Fatigue Cracks, The Metallurgical Society, Inc., Warrendale, PA, 1986, pp. 427-452.

[18] Swain, M. H., Everett, R. A., Newman, J. C., Jr. and Phillips, E. P., "The Growth of Short Cracks in 4340 Steel and Aluminum-Lithium 2090," *AGARD R-767*, 1990, pp. 7.1-7.30.

[19] Miller, K. J., "The Behavior of Short Fatigue Cracks and their Initiation," *Fatigue and Fracture of Engineering Material and Structures*, Vol. 10, 1987, pp. 93-113.

[20] El Haddad, M. H., Dowling, N. E., Topper, T. H. and Smith, K. N., "J Integral Application for Short Fatigue Cracks at Notches," *International Journal of Fracture.*, Vol. 16, 1980, pp. 15-30.

[21] Newman, J. C., Jr., " A Nonlinear Fracture Mechanics Approach to the Growth of Small Cracks," Behavior of Short Cracks in Airframe Components, Zocher, H., ed., *AGARD CP-328*, 1983, pp. 6.1-6.26.

[22] Forth, S. C., Newman, J. C., Jr. and Forman, R. G., "On Generating Fatigue Crack-growth Thresholds," *International Journal of Fracture*, Vol. 25, 2003, pp. 9-15.

[23] Newman, J. C., Jr., Schneider, J., Daniel, A. and McKnight, D., "Compression Pre-cracking to Generate near Threshold Fatigue-Crack-Growth Rates in Two Aluminum Alloys," *International Journal of Fracture*, Vol. 27, 2005, pp. 1432-1440.

[24] Schijive, J., "The Practical and Theoretical Significance of Small Cracks - An Evaluation," Fatigue 84, EMAS, Ltd., 1984, pp. 751-771.

[25] Lankford, J., "The Growth of Small Fatigue Cracks in 7075-T6 Aluminum," *Fatigue of Engineering Materials and Structures*, Vol. 6, 1983, pp. 15-32.

[26] Lankford, J., "The Effects of Environment on the Growth of Small Fatigue Cracks," *Fatigue of Engineering Materials and Structures*, Vol. 6, 1983, pp. 15-32.

[27] Suresh, S. and Ritchie, R. O., "A Geometric Model for Fatigue Crack Closure Induced by Fracture Surface Roughness," *Metallurgical and Material Transactions*, Vol. 13A, 1982, pp. 1627-1631.

[28] Barter, S. A., Sharp, P. K., Holden, G. and Clark, G., "Initiation and Early Growth of Fatigue Cracks in an Aerospace Aluminum Alloy," *Fatigue and Fracture of Engineering Material and Structures*, Vol. 25, 2002, pp. 111-125.

[29] Walker, K. F. and Barter, S. A., "The Critical Importance of Correctly Characterizing Fatigue Crack-growth Rates in the Threshold Regime," Int. Cong. Aero. Fatigue, 26th ICAF Symposium, 2011.

[30] Newman, J. C., Jr., Yamada, Y. and Newman, J. A., "Crack-Closure Behavior of 7050 Aluminum Alloy near Threshold Conditions for Wide Range in Load Ratios and Constant K_{max} Tests," *Journal of ASTM International*, Vol. 7, No. 4, 2010.

[31] FALSTAFF - A Description of Flight Aircraft Standard for Fatigue Evaluation, Combined Report of F&W (Switzerland), LBF (Darmstadt), NLR (Amsterdam) and IABG (Munich), 1976.

[32] Murakami, Y. (editor), "The Rainflow Method in Fatigue," International Symposium Fatigue Damage Measurement and Evaluation under Complex Loadings, Fukuoka, Japan, 1991.

[33] de Jonge, J. B., Schutz, D., Lowak, H. and Schijive, J., "A Standardized Load Sequence for Flight Simulation Tests on Transport Aircraft Wing Structures," LBF-Bericht FB-106, NLR TR 73029 U, 1973.

[34] Lowak, H., de Jonge, J. B., Franz, J. and Schutz, D., "MINITWIST: A Shortened Version of TWIST," LBF-Bericht FB-146, Laboratorium fur Betriebsfestigkeit, 1979.

[35] Yamada, Y., Ziegler, B. and Newman, J. C., Jr., "Application of a Strip-Yield Model to Predict Crack-growth under Variable-Amplitude and Spectrum Loading - Part 1: Compact Specimens," *Engineering Fracture Mechanics*, Vol. 78, 2011, p. 2597.

[36] Ziegler, B., *Fatigue and Fracture Testing and Analysis on Four Engineering Materials*, Ph.D Thesis, Mississippi State University, 2011.

[37] Yamada, Y., *Experimental Investigations on Near Threshold Events on Fatigue Crack Growth*, Ph.D Thesis, Mississippi State University, Mississippi State University, 2009.

[38] Dugdale, D. S., "Yielding of Steel Sheets Containing Slits," *Journal of Mechanics and Physics of Solids*, Vol. 8, No.2, 1960, pp. 100-104.

[39] Dill, H. and Saff, C., "Spectrum Crack-growth Prediction Method based on Crack Surface Displacement and Contact Analyses," *ASTM STP 595*, 1976, pp. 306-319.

[40] Newman, J. C., Jr., "A Crack-Opening Stress Equation for Fatigue Crack-growth," *International Journal of Fracture*, Vol. 24, 1984, R131-R135.

[41] Elber, W., "Crack Closure and Crack-growth Measurements in Surface-Flawed Titanium Alloy Ti-6Al-4V," *NASA-TN-D-8010*, 1975.

[42] Yamada, Y. and Newman, J. C., Jr., "Crack Closure under High Load-Ratio Conditions for Inconel-718 near Threshold Conditions," *Engineering Fracture Mechanics*, Vol. 76, 2009, pp.209-220.

[43] Yamada, Y. and Newman, J. C., Jr., "Crack-Closure Behavior of 2324-T39 Aluminum Alloy near Threshold Conditions for High Load Ratio and Constant K_{max} Tests," *International Journal of Fracture*, Vol. 31, 2009, pp. 1780-1787.

[44] Donald, J. K., "A Procedure for Standardizing Crack Closure Levels," *ASTM STP 982*, American Society for Testing and Materials, Philadelphia, PA, pp. 222-229, 1988.

[45] Standard Test Method for Measurement of Fatigue Crack-growth rates, *ASTM E-647*, American Society for Testing and Materials, 2009.

[46] White, P., Barter, S. and Molent, L., "Observations of Crack Path Changes Caused by Periodic Underloads in AA 7050-T7451," *International Journal of Fracture*, 2007.

[47] Hudson, M. C., "Effect of Stress Ratio on Fatigue-Crack-growth in 7075-T6 and 2024-T3 Aluminum-Alloy Specimens, *NASA-TN-D-5390*, 1969.

APPENDIX A

FASTRAN VERSION 3.82SP USER GUIDE

(Refer to NASA TM-104159 [6] for explanations of most parameters. Additional parameters are described herein. Free format unless otherwise noted.)

FASTRAN Input File:

1. Problem Title

   READ TITLE

   FORMAT (20A4)

2. Spectrum Filename

   READ SPECTRA

   FORMAT (20A4)

3. Material Title

   READ MAT

   FORMAT (20A4)

4. Material Tensile Yielding Properties

   READ SYIELD, SULT, E, ETA, ALP, NALP, NEP, BETA

5. Fatigue-Crack-growth Rate Option

   READ IRATE

   Repeat lines 6 to 7 IRATE times (J = 1 to IRATE).

6. Fatigue-Crack-growth Rate Equation and Fracture Properties

   READ C1(J), C2(J), C3(J), C4(J), C5(J), C6(J), KF, M

   (Note: C6 is power on the [1-(Kmax/C5)^C6] term in equation 15.)

7. Fatigue-Crack-growth Rate Table

   (a) READ NTAB, NDKTH

(Set NDKTH = 0 for current code or see comments about NDKTH

in comment section near the top of the fastran3x.f code)

If NTAB = 0, go to line 8, otherwise continue:

(b) READ DKETAB(I,J), CGRTAB(I,J)

Repeat line 7(b) NTAB times.

8. Crack-growth Rates at Transition (NALP = 1 option only)

READ RATE1, ALP1, BETA1, RATE2, ALP2, BETA2

9. Date Output Options

READ NIPT, NPRT, LSTEP, NDKE, DCPR

10. Specimen Type and Loading

READ NTYP, LTYP, LFAST, NS, NFOPT, INVERT, KCONST

[Note: NTYP = -13, -12, 7 and 8 are not described in NASA

TM-104159, see comments at top of fastran3x.f code.

NTYP = 99 and -99 are user input crack configurations.

A new table format has been incorporated for NTYP = -99.

This option is for cracks from holes. Table input is

crack length measured from edge of hole,c, divided by width,

c/W (input width, W, in line 11) against fc. Thus,

K = S (pi c)^1/2 fc and fastran3x.f converts to c'/W

against Fc, where c' = RAD + c.]

11. Specimen and Crack Starter-Notch Dimensions

READ W, T, CI, AI, CN, AN, HN, RAD

12. Stress-Intensity Factor Table or Equation (NTYP = 99 & -99 only)

(a) READ KTAB

If KTAB = 0, go to line 13, otherwise continue:

(b) READ CWTAB(I), FCTAB(I)

Repeat line 12(b) KTAB times.

(Note: KTAB = 0 is user input equation in Subroutine SIF99.

KTAB > 0 is user input table in the form of c/w

against Fc (CWTAB(I) and FCTAB(I), respectively,

I = 1 to KTAB). Maximum KTAB = 50.)

13. Final Crack Length Requested

READ CF

14. Special Input for Various Crack Configurations

(a) If NTYP = 0 or 7 (with LTYP = 2) or NTYP = -10 then:

READ GAMMA

(b) If NTYP = -7, -8 and -9 then:

READ XKT, NBCF

(c) If NTYP = 5 then:

READ RADIUS

(d) If NTYP = -12 or 13

READ RIVETS, RLF1, RLF2, WR, WJ, NODKL, GAMMA, DELTA

(Note: NTYP = -13, -12 and 7 require special input that is not

described in current NASA manual, see comments in fastran3x.f.)

15. Input Constant-Amplitude Loading to Initiate Crack from Starter Notch

READ SMAX, SMIN

16. Special Input for Proof Test or Constant Crack-Opening Stress Concept

READ NRC, DVALUE

17. Input Primary Fatigue Loading

(a) Constant- or Variable-Amplitude Loading (NFOPT = 0 or 1):

Line 1: READ MAXSEQ, MAXBLK, LPRINT, MAXLPR

LPRINT = MAXLPR = 0

Line 2: READ SCALE

Line 3: READ NBLK, NSL(I), NSQ(I)

Line 4: READ SMAXP(I,J), SMINP(I,J), NCYCP(I,J)

Repeat lines 3 and 4, MAXBLK times.

B. TWIST [14] or MINI-TWIST [15] Flight-Load Sequence

(NFOPT = 2 or 3, respectively):

Line 1: READ MAXSEQ, MAXBLK, LPRINT, MAXLPR

MAXSEQ = 4000 MAXBLK = 10

LPRINT = 0, 1 or 2

Line 2: READ SMEAN

C. FALSTAFF [16] Flight-Load Sequence (NFOPT = 4):

Line 1: READ MAXSEQ, MAXBLK, LPRINT, MAXLPR

MAXSEQ = MAXBLK = 200

LPRINT = 0, 1 or 2

Line 2: READ SPEAK

D. Space Shuttle (STS/NLR) Load Sequence (NFOPT = 5):

(SPECTRA = stsn)

Line 1: READ MAXSEQ, MAXBLK, LPRINT, MAXLPR

MAXSEQ = MAXBLK = MAXLPR = 2

LPRINT = 0 or 1

Line 2: READ SPEAK

E. Gaussian Load Sequence [17] (NFOPT = 6):

Line 1: READ MAXSEQ, MAXBLK, LPRINT, MAXLPR

MAXSEQ = MAXBLK = 839

LPRINT = 0 or 1

Line 2: READ SPEAK, SMEAN

F. Felix/28 [18] Helicopter Load Sequence (NFOPT = 7):

Line 1: READ MAXSEQ, MAXBLK, LPRINT, MAXLPR

MAXSEQ = 140 MAXBLK = 12

LPRINT = 0, 1 or 2

Line 2: READ SPEAK

G. Spectrum Read from List of Stress Points (NFOPT = 8):

Line 1: READ MAXSEQ, MAXBLK, LPRINT, MAXLPR

MAXSEQ = MAXBLK = NPOINTS/5000 + 1

LPRINT = 0, 1 or 2

Line 2: READ SPEAK

H. Spectrum Read from Flight-by-Flight Input (NFOPT = 9):

Line 1: READ MAXSEQ, MAXBLK, LPRINT, MAXLPR

MAXSEQ = MAXBLK = NFLIGHTS

LPRINT = 0, 1 or 2

Line 2: READ SPEAK

I. Spectrum Read from Flight Schedule Input (NFOPT = 10):

Line 1: READ MAXSEQ, MAXBLK, LPRINT, MAXLPR

MAXSEQ = Total number of flights in schedule

MAXBLK = Number of different flights

LPRINT = 0, 1 or 2

MAXLPR = Number of flights to be printed out

Line 2: READ SPEAK

18. Input Variables for Load-Reduction Threshold Test

READ KTH, SMAXTH, RTH, CONST, PRT

(New option added for KTH = 4 -- KMAX = constant

and new parameter PRT added for KTH = 3 option,

see comments about KMAX test in comment section

near the top of the fastran3x.f code.

New option added for KTH = 5 -- CMOD = constant

Wu's load-reduction threshold method)

19. Input HALT or next problem (lines 1 to 18).